Acta Geologica Polonica, Vol. 70 (2020), No. 1, pp. 51–78
DOI: 10.24425/agp.2019.126453

Dawsonite as an indicator of multistage deformation and fluid pathways within fault zones: Insights from the Fore-Dukla Thrust Sheet, Outer Carpathians, Poland

BARBARA RYBAK-OSTROWSKA[1]*, ARKADIUSZ GĄSIŃSKI[2] and GRZEGORZ KAPROŃ[1]

[1] *Faculty of Geology, University of Warsaw, Żwirki i Wigury 93, 02-089 Warsaw, Poland.*
[2] *Institute of Ceramics and Building Materials, Postępu 9, 02-676 Warsaw, Poland.*
** Corresponding author: barbara.rybak@uw.edu.pl*

ABSTRACT:

Rybak-Ostrowska, B., Gąsiński, A. and Kaproń, G. 2020. Dawsonite as an indicator of multistage deformation and fluid pathways within fault zones: Insights from the Fore-Dukla Thrust Sheet, Outer Carpathians, Poland. *Acta Geologica Polonica*, **70** (1), 51–78. Warszawa.

The structural pattern developed within metre to microscopic scale thrust and strike-slip fault zones exposed in the Palaeogene flysch rocks of the Fore-Dukla Thrust Sheet in the south-eastern part of the Silesian Nappe, Outer Carpathians, Poland, reveals evidence for upper crustal deformation and fluid flow. Syntectonic dawsonite [$NaAlCO_3(OH)_2$] indicates the following series of deformational events within the fault zones: i) detachment and buckle folding resulting from movement along thrust faults; ii) faulting as a compensation of the shortening, resulting in the fault propagation folding, breakthrough thrust faulting and imbrications; and iii) strike-slip faulting. The microstructural pattern coupled with the growth of a related sequence of carbonate minerals within the fault zones, followed by present-day dawsonite precipitation and tufa formation, indicate a continuing influence of fluids within the Silesian Nappe up to and including modern time. Structural observations at metre to microscopic scales coupled with EDS mapping of rocks indicate that dawsonite is a unique tool for the reconstruction of subsequent deformation in the Fore-Dukla Thrust Sheet.

Key words: Syntectonic dawsonite; Fault zone; Multistage development; Fluid pathways; Outer Carpathians.

INTRODUCTION

The occurrence of dawsonite [$NaAlCO_3(OH)_2$] in natural settings is well known from sedimentary rocks in different localities worldwide (Stevenson and Stevenson, 1965; Baker *et al.* 1995; Ferrini *et al.* 2003; Worden 2006; Zalba *et al.* 2011). Dawsonite is present in oil shales and natural carbon dioxide reservoirs (Smith and Milton 1966; Kamilli and Ohmoto 1977; Moor *et al.* 2005; Kharaka *et al.* 2006; Okuyama 2014; Palayangoda and Nguyen 2015; Kiràly *et al.* 2016; Li and Li 2017), and coal (Golab *et al.* 2006; Ming *et al.* 2017). It is also known from fluid inclusions in hydrothermal minerals (McLaughlin *et al.* 1985; Sirbescu and Nabelek 2003). In the last two decades dawsonite has been the subject of extensive studies related to carbon dioxide storage in subsurface sedimentary formations (Knauss *et al.*, 2005; Worden 2006; Liu *et al.* 2011; Wigley *et al.* 2012; Trémosa *et al.* 2014; Estublier *et al.* 2017). Thus, as a mineral trap of CO_2, dawsonite has become the object of geochemical modelling, laboratory synthesis and experiments (e.g. Johnson *et al.*, 2004; Zerai *et al.* 2006; Bénézeth *et al.* 2007; Stoica and Pèrez-Ramírez 2010; Yu *et al.* 2016).

Although dawsonite is well-known from dif-

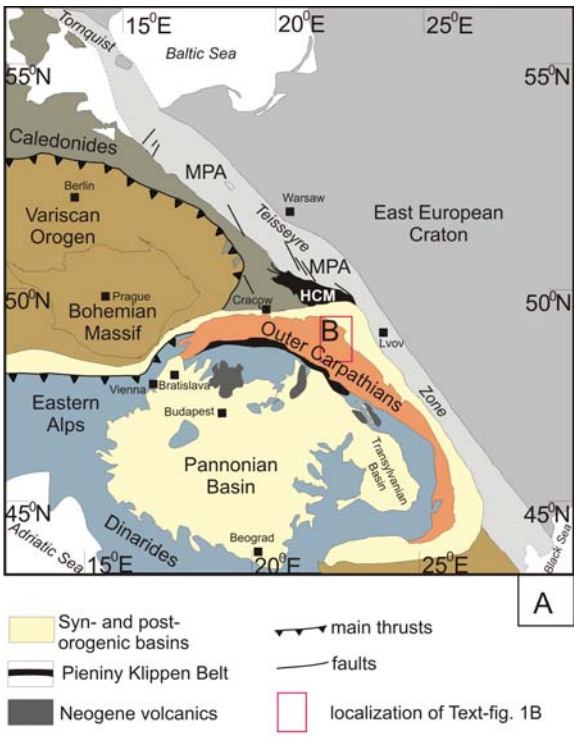

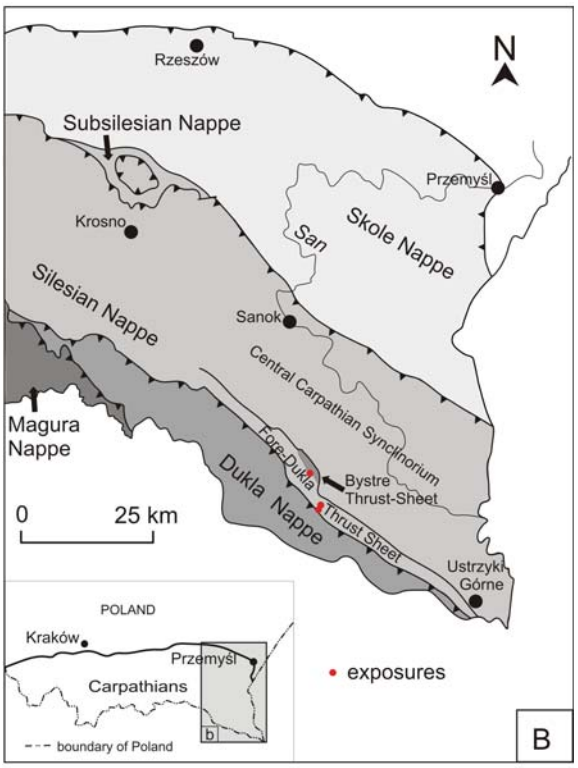

Text-fig. 1. Location of the study area. A – Tectonic sketch-map of Central Europe (simplified after Guterch *et al.*, 2000); MPA – Mid-Polish Anticlinorium, HCM – Holy Cross Mountains. B – Tectonic sketch-map of the eastern part of the Outer Carpathians in Poland (simplified after Żytko et al. 1989)

ferent geological environments, its tectonic origin and/or involvement have been scarcely recognised (e.g. Ferrini *et al.* 2003). The present study focuses on dawsonite veins locally associated with dolomite–ankerite–calcite veins found within the fault zones in a narrow south-eastern part of the Silesian Nappe in Poland – the Fore-Dukla Thrust Sheet (Text-fig. 1).

Several decades of studies on fault zones indicate that upper crustal deformation of rocks is dominated by brittle failure, resulting in fault rocks formation along with subsidiary faulting and fracturing, and their sealing (Sibson 1977, 1983; Scholz 1988, 2002). Distribution of subsidiary structures within fault zones is related to their internal architecture including two components: the core and the damage zone (e.g. Chester *et al.* 1993; Caine *et al.* 1996). Field and core studies along with experimental works indicate that the lithological differences of the rock series define characteristic structural features and patterns (Chester 1996, 2003; Morley 1994; Erickson 1996; Fischer and Jackson 1999; Ferrill and Morris 2008). An additional factor governing the development of structures is diagenesis, which results in the evolution of the mechanical properties of rocks during deformation (Donath 1964; Knipe 1993; Shackleton *et al.* 2005; Laubach *et al.* 2009). Fault and fracture networks propagate along or across lithological units (Odling *et al.* 1999; Sibson 1996; 2003; Eichhubl and Boles 2000; Van Noten *et al.* 2012) that may play a dual role as barriers or pathways for fluid flow (Arndt *et al.* 2014). Competence contrasts of rocks within fold and thrust belts promote buckling, detachment folding and thrust faulting (Ramsay 1967; Dahlstorm 1969, 1990; Jamison, 1987; Mastella 1988; Fischer and Jackson 1999; Latta and Anastasio 2007; Hayes and Hanks 2008). A rhythmic siliciclastic sequence within the Fore-Dukla Thrust Sheet provides macro- and microstructural evidence for the process of rock deformation within fault zones. The brittle deformation mechanism is primarily cataclastic within thrust fault zones, whereas strike-slip fault zones are dominated by fracturing and associated veining. Microscopic evidence coupled with EDS mapping provide insights into the micromechanics of damage accumulation and failure of host rocks, followed by mineral healing during different deformational stages of the Fore-Dukla Thrust Sheet. Based on the assembled data and recent studies on active and exhumed fault zones coupled with experimental data, we discuss the structural pattern of thrust and strike-slip fault zones and related mineral infilling

to shed light on the process of rock deformation in relation to mineral precipitation within fault zones of the Fore-Dukla Thrust Sheet. The results of this study are a step toward the understanding of the complex architecture and cementation patterns of fault zones in the Outer Carpathians, which are crucial for predicting the contemporary potential seal behaviour of fault zones.

GEOLOGICAL SETTING

The Fore-Dukla Thrust Sheet is located in the eastern part of the thin-skinned Outer Carpathians Fold and Thrust Belt (OCFTB, Text-fig. 1). The OCFTB forms an accretionary wedge that originated during the collision of the Alcapa and Tisza-Dacia microplates with the North European plate (Książkiewicz 1972; Oszczypko and Tomaś 1985; Csontos *et al.* 1992; Royden 1998; Fodor *et al.* 1999). It comprises stacked nappes built of Upper Jurassic to Lower Miocene rocks (Żytko *et al.* 1989; Jankowski *et al.* 2004), mainly of flysch origin (Oszczypko 1998). The rocks have been diachronously folded and thrusted from late Oligocene to middle Miocene time (e.g. Burchfiel and Royden 1982; Kováč *et al.* 1998; Oszczypko 2004, 2006; Nemčok *et al.* 2006), with progressive imbrications of Silesian series in early Miocene time (e.g. Gągała *et al.* 2012). Major thrusts accommodate variable displacements, e.g., a minimum of 27 km for the Magura Nappe within the Mszana Dolna Window (Mastella 1988), a maximum of 55 km for the Magura Nappe on the Dukla Nappe, and 19 km of the Silesian Nappe on the Skole Nappe (Gągała *et al.* 2012).

The dawsonite veins occur within rocks exposed along the fault zones located in the Fore-Dukla Thrust Sheet (Text-fig. 1B), within the southernmost part of the Silesian Nappe (Opolski 1933; Świdziński 1958; Rubinkiewicz 2007), in the foreland of the Dukla Nappe (Ślączka 1971). To the north-east the Fore-Dukla Thrust Sheet borders the Central Carpathian Synclinorium (Text-fig. 1B) (Tołwiński 1933; Kuśmierek 1979; Mastella 1995, Rubinkiewicz 2007). The Dukla thrust dips southwards with angles that range from 45º to 70º (Rubinkiewicz 1996). It is steep in relation to the regional trend of thrusting within the OCFTB, e.g. 6–19º of the Magura thrust in the Mszana Dolna Window (Mastella 1988), and 20–40º in the Beskid Wyspowy Mts. (Konon 2001).

The Fore-Dukla Thrust Sheet comprises Lower Cretaceous to Oligocene flysch deposits (Ślączka 1957, 1958; Ślączka and Żytko 1978; Kuśmierek 1979; Gucik and Wójcik 1982; Haczewski *et al.* 2000; Oszczypko 2006) with the oldest strata exposed within the northernmost part, in the minor Bystre Thrust Sheet (Ślączka 1959, 1968). The thickness of the rock sequence is estimated at 3.7 km (Kuśmierek 1979). The estimated burial depth for the Fore-Dukla Thrust Sheet varies from 6–8 km (Świerczewska 2005) to 3.6–8.6 km (Andreucci *et al.* 2013), based on surface paleo-temperatures combined with recent thermal gradients. However, Hurai *et al.* (2006) estimated a burial of even 11 km in the adjacent Dukla Nappe, based on trapping *PT* conditions calculated from fluid inclusions in quartz.

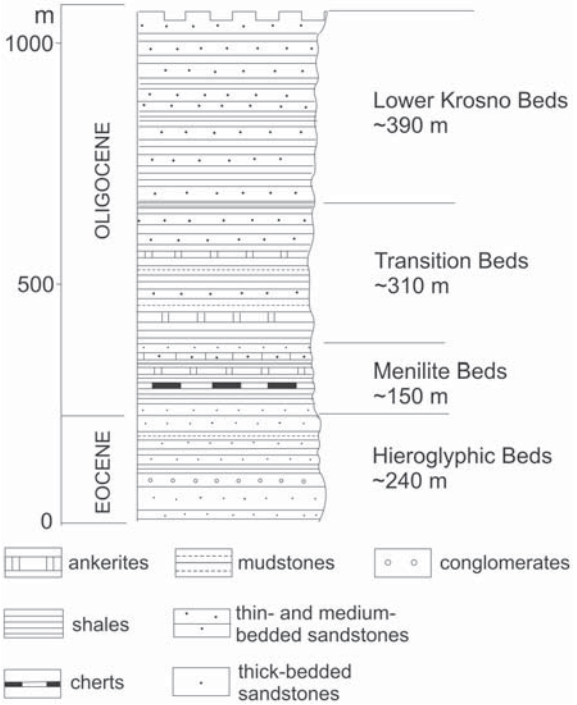

Text-fig. 2. Generalized lithostratigraphic succession of the Silesian series in the study area (after Ślączka 1959; Kuśmierek 1979, modified)

The present study focuses on the Silesian series, which comprise the following informal litostratigraphic units: Hieroglyphic, Menilite, Transition and Krosno beds (Text-fig. 2). The flysch series were deposited in a deep marine environment within the Carpathian Basin of north-western Tethys (e.g. Poprawa *et al.* 2002; Oszczypko 2004). The Hieroglyphic Beds include Eocene turbiditic deposits, embracing thin- and medium-bedded fine-grained sandstones with intercalations of green and calcareous or black siliceous shales. The Menilite Beds consist

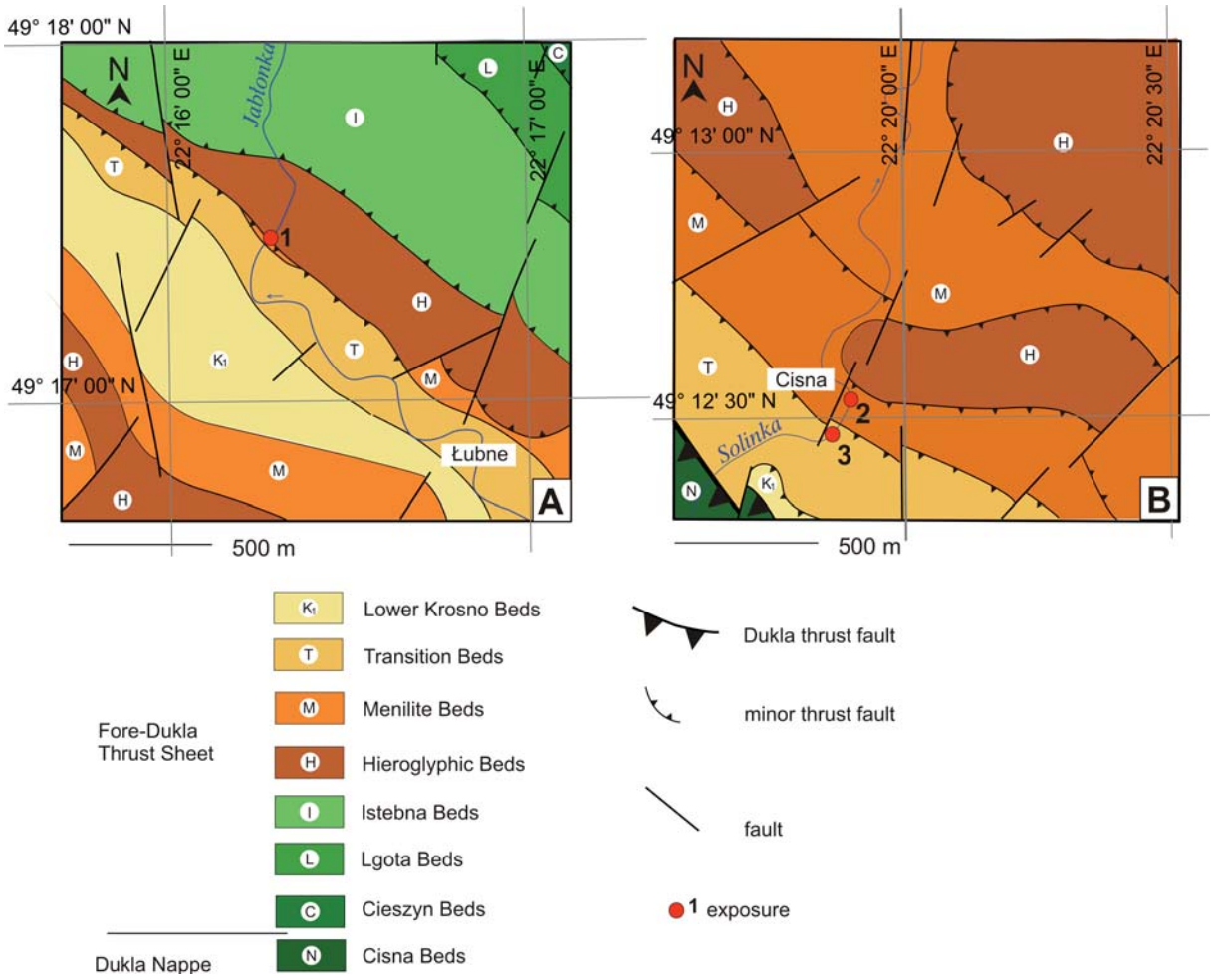

Text-fig. 3. Location of exposures on a tectonic sketch-maps (after Mastella 1995, modified). A – Łubne region. B – Cisna region

of Oligocene hemipelagic black siliceous and grey clayey shales alternating with thin-bedded turbiditic fine-grained calcareous sandstones and ankerites. They are considered source rocks with high petroleum potential (Kotarba and Koltun 2006). The Transition Beds comprise Oligocene rocks that are characteristic of both Menilite and Krosno beds, i.e. grey and brown-grey clayey or calcareous shales, thin- to medium-bedded, fine-grained sandstones and grey mudstones alternating with black siliceous shales and occasionally with ankerites. Such a variation in rock type reflects the transition from hemipelagic and/or distal flysch sedimentation recorded by the Menilite Beds (e.g. Köster *et al.* 1998) to synorogenic proximal flysch formation recorded by the Krosno Beds (Jucha and Kotlarczyk 1961; Pescatore and Ślączka 1984; Poprawa *et al.* 2002; Bojanowski 2007).

The Fore-Dukla Thrust Sheet comprises a series of folded slices that are separated by map-scale NW–SE-trending thrusts (Text-fig. 3). The slices have a steep position, laterally overlapping one another, or are cut by transversal faults (Mastella 1995; Haczewski *et al.* 2000). Bedding dips in the Fore-Dukla Thrust Sheet are variable near the Dukla thrust, in the central part, and to the north near the contact with the Central Carpathian Synclinorium (Rubinkiewicz 1996, 2007). NW to SE-trending fold axes are mainly subhorizontal but within the central part of the Fore-Dukla Thrust Sheet the trend changes (Mastella 1995; Rubinkiewicz 1998).

Three sets of faults cut the Fore-Dukla Thrust Sheet (e.g. Mastella and Szynkaruk 1998); i) and ii) are strike-slip faults forming a conjugate system that originated during the middle and late Miocene af-

ter nappe formation. They were partly reactivated as normal faults during post-thrusting extension. Set iii) comprises predominantly normal faults that originated during the post-thrusting extension in the Neogene (e.g. Mastella and Szynkaruk 1998; Rubinkiewicz 2000). Following Andreucci *et al.* (2013), extensional tectonics was active between 10–7 Ma prior to or during the major exhumation stage in the eastern Outer Carpathians.

METHODS

Fieldwork at a scale of 1:25000 resulted in the identification of a few minor fault zones mineralised by dawsonite. Although the fieldwork was hampered by infrastructural development near villages and rather accumulative tendency of the streams, at least three exposures were found to provide structural and mineral data for this study. Swift currents of streams and poor exposures have allowed for field documentation predominantly on sketches, with photographs of small-scale structures made in a few places. Samples of slickensides were collected mainly from minor thrusts and subsidiary faults, and strike slip faults. The lithology of rocks and their damage within the fault zones caused samples to be susceptible to disintegration during collection and thin section preparation. Hence, the thin sections were of variable quality. All thin sections were cut parallel to the mineral lineation observed on the fault planes.

Microstructural analysis was performed on polarised microscope and scanning electron microscope images. The polarised microscope images were obtained by a Nikon Eclipse LV 100POL microscope equipped with a scanning table. The acquisition of images was performed using the NIS ELEMENTS software. The scanning electron microscope images were obtained using a Zeiss Sigma VP® microscope at an accelerating voltage of 20 kV, aperture of 120 mm and angular selective BSE detector. The system was equipped with two XFlash® 6 | 10 EDS detectors, which enabled the getting of a good signal over 100k counts per second. The acquisition was performed using the Bruker Esprit® software. For every BSE image, a set of element maps was obtained with the so-called hyper-mapping option. The acquired image files were combined into final output images for every signal by a stitching process described by Preibisch *et al.* (2009), using a Fiji distribution of the ImageJ software (Schindelin *et al.* 2012). Later, the procedure of subtracting and adding of signals was performed in order to obtain a map of minerals.

The quantification of chemical phases was based on EDS mappings supported by BSE images. Thus, porosity and unrecognised phases were not included into the final calculated results, which were normalised to 100%.

X-ray diffraction (XRD) analyses of 8 selected samples were performed to identify the mineral composition of veins. Mineral samples were analysed on the powder diffractometer X'Pert-PRO MPD with a DSH method using monochromatic Co K-a radiation at a 40 mA current and 40 kV voltage. The analyses applied the capillary diameter of 0.3 mm for samples no 1, 2, 3, 6, 7, and 0.5 mm for sample 4. Detection of radiation was provided by a PIXcel line detector. The measurement conditions were as follows: start position [°2Q] 5.0, end position [°2Q] 90.0, step size [°2Q] 0.026, generator settings 40 mA, 40 kV, time of measurement 2 h 34 min.

FIELD OBSERVATIONS

Dawsonite assemblages were noted for the first time in the Fore-Dukla Thrust Sheet by Rybak (2005). The exposures with dawsonite host also calcite and/or ankerite veins along with marmarosh diamonds, i.e. quartz with a perfect euhedral habit.

Minor fault zones with dawsonite veins are exposed in the central and southern part of the Fore-Dukla Thrust Sheet (Text-figs 1B, 3A, B). The first exposure is separated from the second and third by about 10 km in a straight line. The distance between the latter two exposures is ca. 180 m. Exposures of the fault zones reach up to 3 m in height and up to a few tens of metres in width. Rocks are strongly deformed and damaged, nevertheless they can be traced across the exposures and the distinct architecture of the fault zones can be followed (Text-figs 4, 5, 6).

The exposure in the Jabłonka Stream (Text-figs 3A, 4A) displays a minor duplex (cf. Rybak, 2005) separated by basal and roof thrusts with a detachment involved along the latter thrust. The major thrusts are listric and show a wavy geometry with dips between 5º and 30ºS. Thrust surfaces are striated and partially highly polished. The main displacement is located along the roof detachment thrust within a decimetre-thick gouge. The thrust separates two generally incompetent rock sequences: the relatively more incompetent Menilite Beds and the relatively more competent Hieroglyphic Beds. Nonetheless, the sequences are in their normal stratigraphic position (Text-figs 2, 4A). The orientation of the thrust changes along the exposure (Text-fig. 4A).

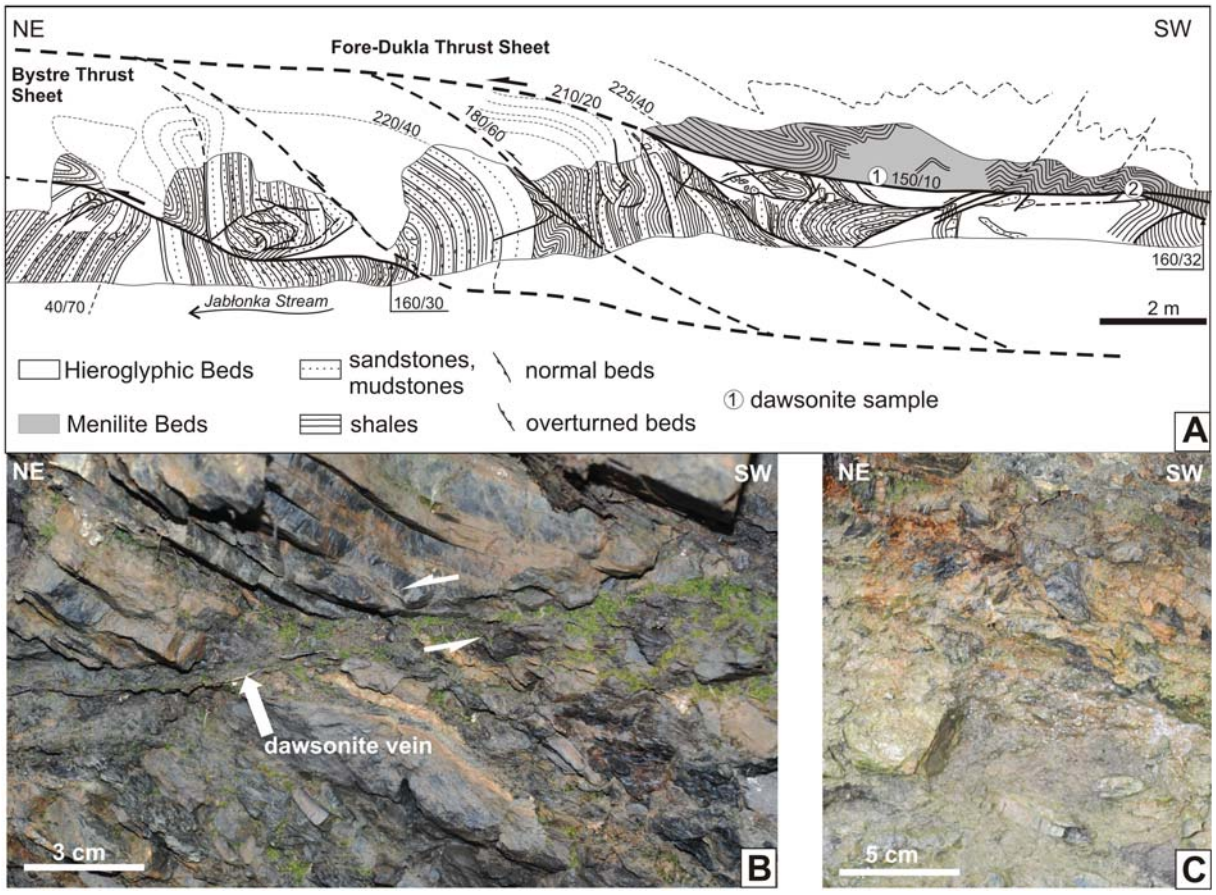

Text-fig. 4. Complex thrust fault zone mineralised with dawsonite exposed in the south-eastern bank of the Jabłonka Stream. A – Tectonic sketch of the outcrop. B – Thrust fault aligned by dawsonite veins. C – Thin cover of tufa on rocks

The basal thrust occurs within the Hieroglyphic Beds and shows a similar orientation as the roof thrust. Dawsonite occurs within the Menilite Beds along the roof thrust and bedding planes in the hanging wall adjacent to the thrust plane (Text-fig. 4A, B).

The structure of the detached incompetent rock succession of the Menilite Beds is interpreted as a detachment box fold (e.g., Mitra 2003). The box fold shows a complex geometry that includes a series of minor second-order chevron folds showing consistent as well as opposite senses of vergence in relation to the sense of movement of the detachment thrust. The highly polished bedding planes lack a mineral lineation. Strikes of the Menilite Beds and the fold axes are partly consistent with the strike of detachment thrust.

The interpreted minor duplex occurs within the Hieroglyphic Beds. The exposure reveals fragments of an imbricate structure involving overlapping sigmoidal slices with folded rock sequences (Text-fig. 4A). The thrusts that separate the slices are subparallel. The spacing of the thrusts is constant and exceeds 3 m. The Hieroglyphic Beds show a variable orientation: overturned in the north-eastern part, changing to normal in the south-western part. Individual slices reveal fragments of folds that are interpreted as open or box folds. The orientation of fold axes is almost consistent with the strikes of the thrust faults. The cores and hinges of folds show complex structures as the result of fold tightening.

The second exposure (Text-fig. 3B) shows a fragment of a minor imbricate structure developed within the upper part of the Menilite Beds (Text-fig. 5). The beds are in a homoclinal arrangement and slightly folded along the thrusts that separate individual slices. The strikes of the beds are sub-parallel to thrust orientations. Steep, north-dipping beds dominate. The thrusts show a variable geometry across the fault zone and define the sigmoidal geometry of the slices

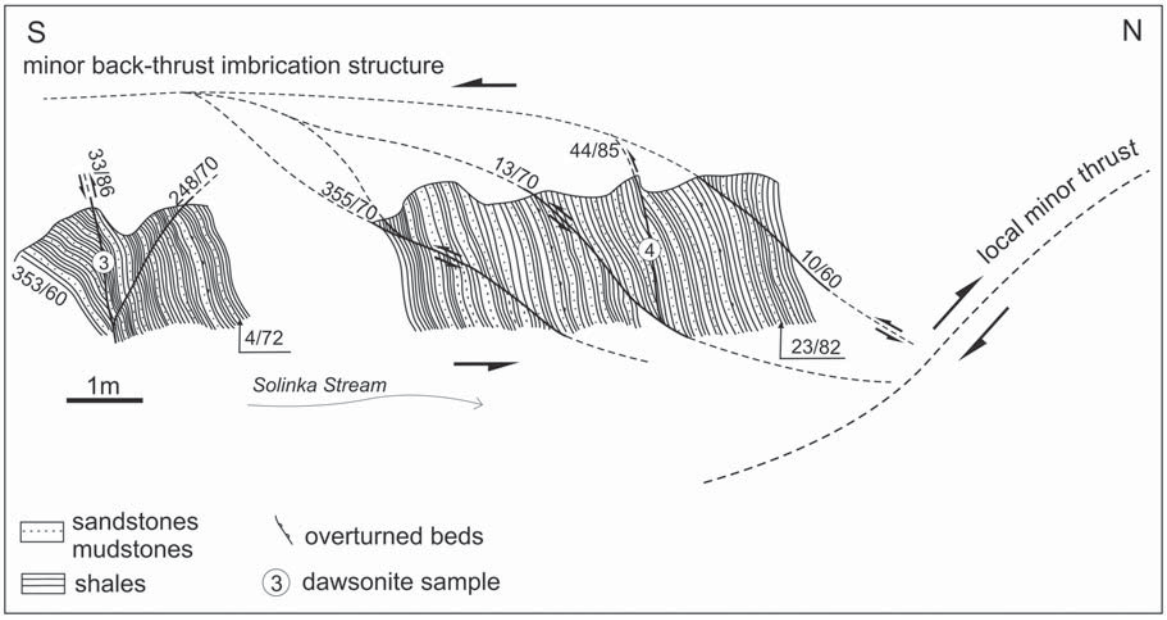

Text-fig. 5. Back-thrust fault zone mineralised by dawsonite exposed in the western bank of the Solinka Stream

(Text-fig. 5). Some of the thrusts branch off, which resulted in the formation of steep, north-east dipping faults and lower order slices. Riedel shears along the faults and incongruous steps on slickensides indicate a reverse component of fault slip. Fault planes oriented nearly parallel to the bedding show multi-layered dawsonite veins associated with thin intercalations of black shales. The minor imbricate structure shows an inclination opposite to the regional trend. Based on field and cartographic data (Text-fig. 3B), the faults can be interpreted as back-thrusts related to the local minor thrust (Text-fig. 5). This issue, however, will be the focus of further studies.

The third exposure reveals a fragment of a complex imbricate structure dissected by a strike-slip fault zone developed within the Transition Beds. The exposure is located in the close vicinity to the frontal part of the Dukla Nappe (Text-figs 3B, 6A). The beds are partly in a homoclinal arrangement and partly folded along the thrusts that separate the individual slices. The strikes of the Transition Beds are sub-parallel to the thrust orientations. Steep and overturned, S-dipping beds dominate. The thrusts show a variable geometry with strikes that vary from 145º to 165º and dips from 10º to 89ºS. Strike-slip faults occur in a few places along the exposure (Text-fig. 6A). They form two sets with steep surfaces that are characterised by strikes at 45–50º (I) and 80–90º (II). Incongruous steps and Riedel shears associated with slickensides indicate sinistral slip along set I and dextral slip along set II. The kinematics and inclination of the faults in relation to regional sinistral strike-slip faults (cf. Rubinkiewicz 1996; Mastella and Szynkaruk 1998) suggest they are second-order P faults within set I and R'_1 faults within set II (Text-fig. 6D).

The bedding and fault planes within the fault zone are covered by fibrous dawsonite (Text-fig. 6B–E). It commonly covers previously formed calcite on fault surfaces or on drusy assemblages (Text-fig. 6C, D).

All exposures show the presence of calcareous tufas represented by thin crusts partly covering rocks within the fault zones (e.g., Text-fig. 4C). Constantly seeping water within the fault zones enables the formation of smooth, thin carbonate covers up to few metres of extent and up to few centimetres in thickness. During several years of fieldwork, formation and erosion of the tufas has been constantly observed (cf. Mastella and Rybak-Ostrowska 2012).

CHARACTERISTICS OF DAWSONITE AND CARBONATE VEIN INFILLING

Macroscopically, dawsonite is primarily fibrous and white in colour with a silky gloss (Text-figs 6B, C, D, 7A, B). XRD analysis identified that the sampled veins are infilled with dawsonite with a small

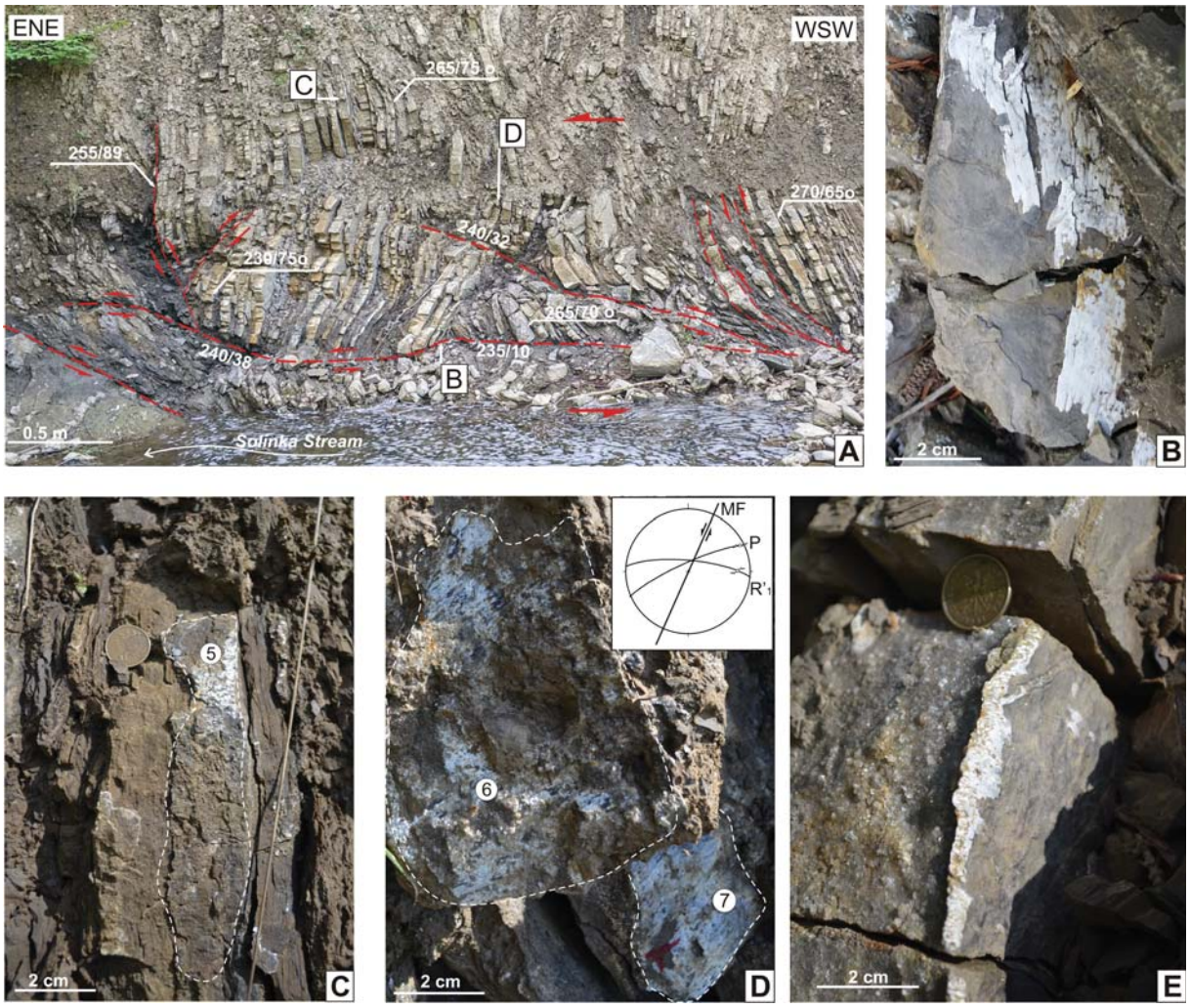

Text-fig. 6. Thrust fault zone cut by strike-slip faults mineralised with dawsonite exposed in the south-eastern bank of the Solinka Stream. A – Localization of strike slip faults along minor imbricated structure. B – Lineation defined by fibrous dawsonite on thrust surface. C, D, E – Examples of slickensides mineralised with fibrous dawsonite

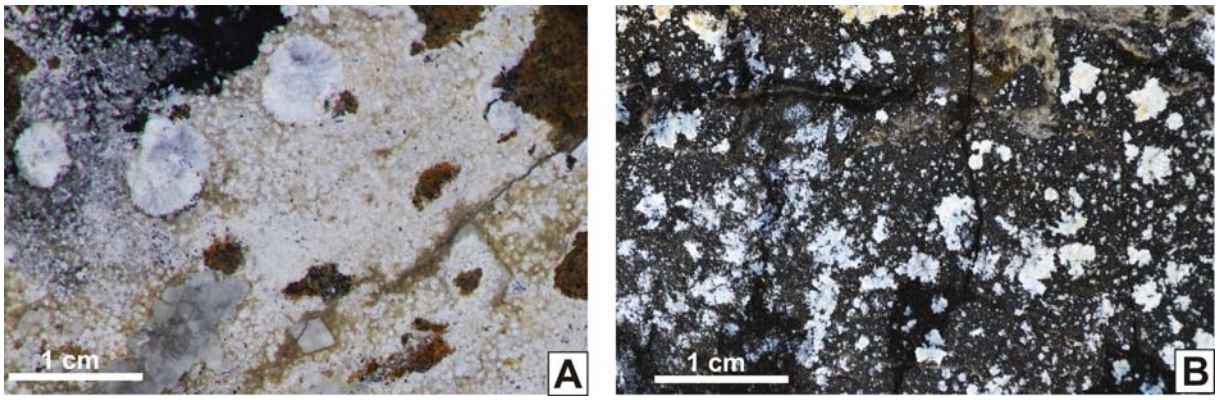

Text-fig. 7. Acicular dawsonite arranged in rosettes on rocks of the Menilite Beds from thrust fault zones. A – Jabłonka Stream, B – Solinka Stream

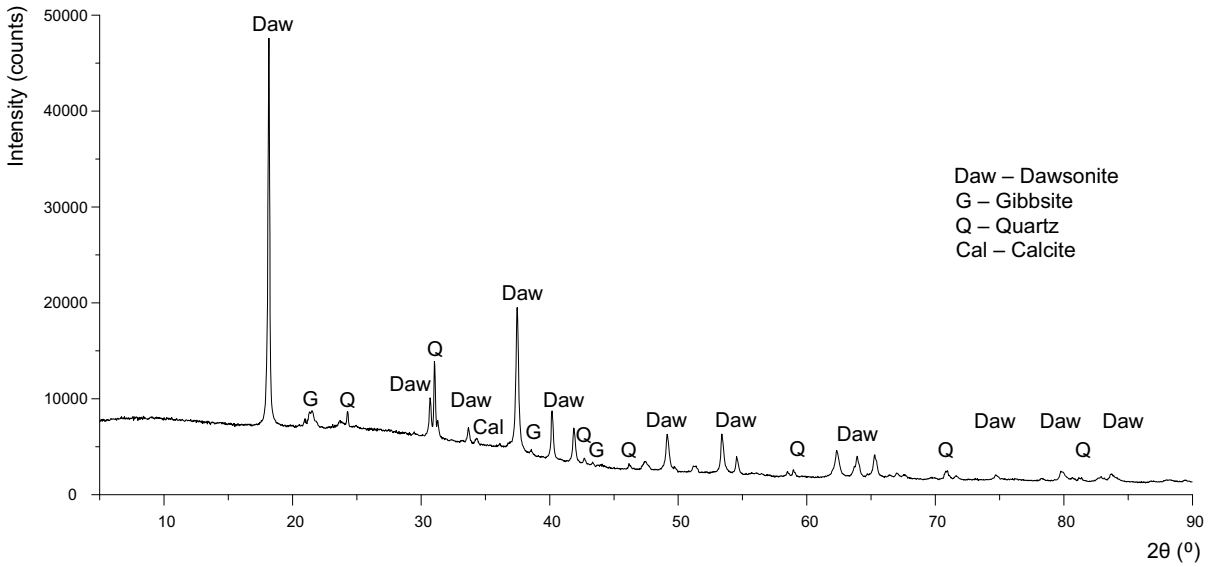

Text-fig. 8. Example of X-ray diffraction analysis of a dawsonite vein sample

admixture of gibbsite [$Al(OH)_3$], calcite [$CaCO_3$] and quartz [SiO_2] (Text-fig. 8). The dawsonite content is about 95% in most of the samples.

Field studies revealed that dawsonite assemblages are localised only within fault zones (e.g., Text-figs 4, 6) and the mineral precipitated during different deformation stages. Dawsonite also forms acicular assemblages that are widespread on host rocks within exposures of fault zones as rosettes up to 6 mm in diameter (Text-fig. 7A, B) or fans up to a few millimetres in size. The observations of selected exposures indicate that dawsonite is capable of present-day seasonal growth and can be destroyed by flood episodes, similarly as tufa deposits.

Macroscopically, the veins are discontinuous, in some parts strongly folded, and of a variable thickness of 1 to 3 mm across the fault zone. The length of the veins reaches up to few tens of centimetres and is limited by the size of exposures. Dawsonite veins occur as single objects or in the form of multi-layered structures. The latter are arranged parallel to each other or display significant small-scale, fault-related folding (e.g. Text-fig. 9A).

Cross-sections parallel to lineation show two types of veins infilled with: i) dawsonite – these veins are closely related to the shale layers of the Menilite Beds and Transition Beds (Text-figs 9, 10, 11A, 12, 13A); and ii) dawsonite associated with dolomite [$CaMg(CO_3)_2$], ankerite [$Ca(Fe,Mg,Mn)(CO_3)_2$], calcite – these veins occur within the mudstones and ankerites of the Transition Beds (Text-figs 13A–E, 14A–C, 15A, B, 16A).

Dawsonite veins show a sub-parallel or oblique arrangement of dawsonite fibres in relation to the vein walls (Text-figs 9B, 10A–E, 12A–D, 13D, 15B). The oblique fibres are slightly curved or sigmoidal in shape, and inclined towards the sense of fold vergence and movement of the sampled fault. The angle of inclination ranges from 15º to 30º.

The boundaries of the vein walls are rough and irregular, especially along veins with an oblique arrangement of the fibres. Cross-sections normal to the sampled veins display an assemblage of host rock inclusions arranged sub-parallel to the vein wall and/or subparallel to the fibres in the outer parts of the veins (Text-figs 10C, 12A, C). They have a longitudinal and lenticular shape or show an irregular appearance. It is likely that the presence of host rock inclusions within the veins stimulated the second order fold development during progressive faulting.

The dawsonite veins from the Menilite Beds contain narrow rims of gibbsite (Text-figs 9C, 11A, 12A, B). The rims reach up to 100 μm in width. The distribution of gibbsite is heterogeneous within the rims. Occasionally, rims of gibbsite cover the fibrous texture of previous dawsonite (Text-fig. 12A, B). Small patches of gibbsite are widespread near the rims and within the veins around the host rock inclusions, as well as within the host rock (Text-fig. 12A, B, C). They are irregular or sub-oval in shape and look like

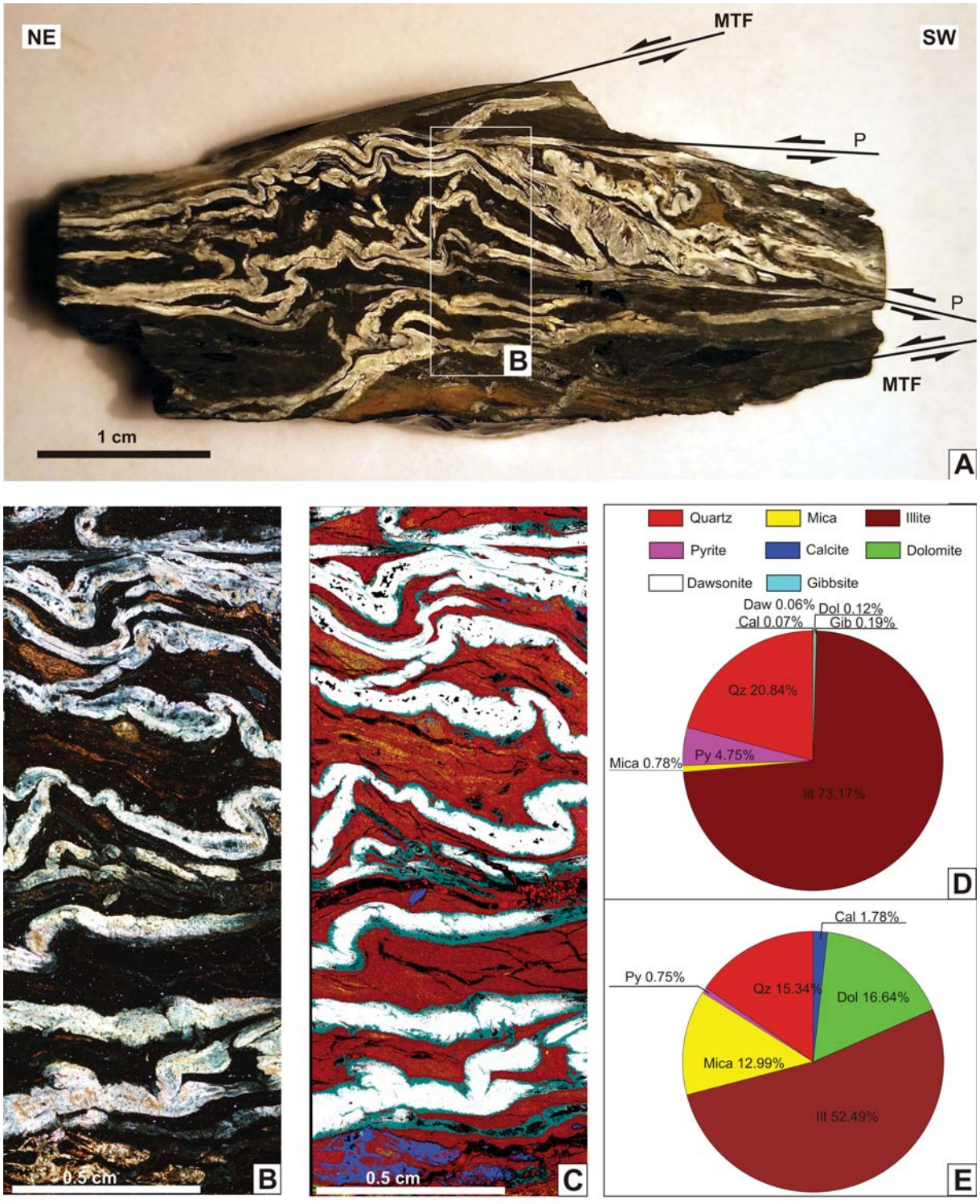

Text-fig. 9. Multi-layered dawsonite veins from the core of a thrust fault zone in the Jabłonka Stream (sample 2). A – Interpretation of small-scale faults within the fault zone. B – BSE image of a selected fragment of multi-layered dawsonite veins. C – EDS map of a selected fragment of multi-layered dawsonite veins. D, E – Mineral composition of rocks within the fault core. Arrows indicate the sense of movement. MTF – main thrust fault

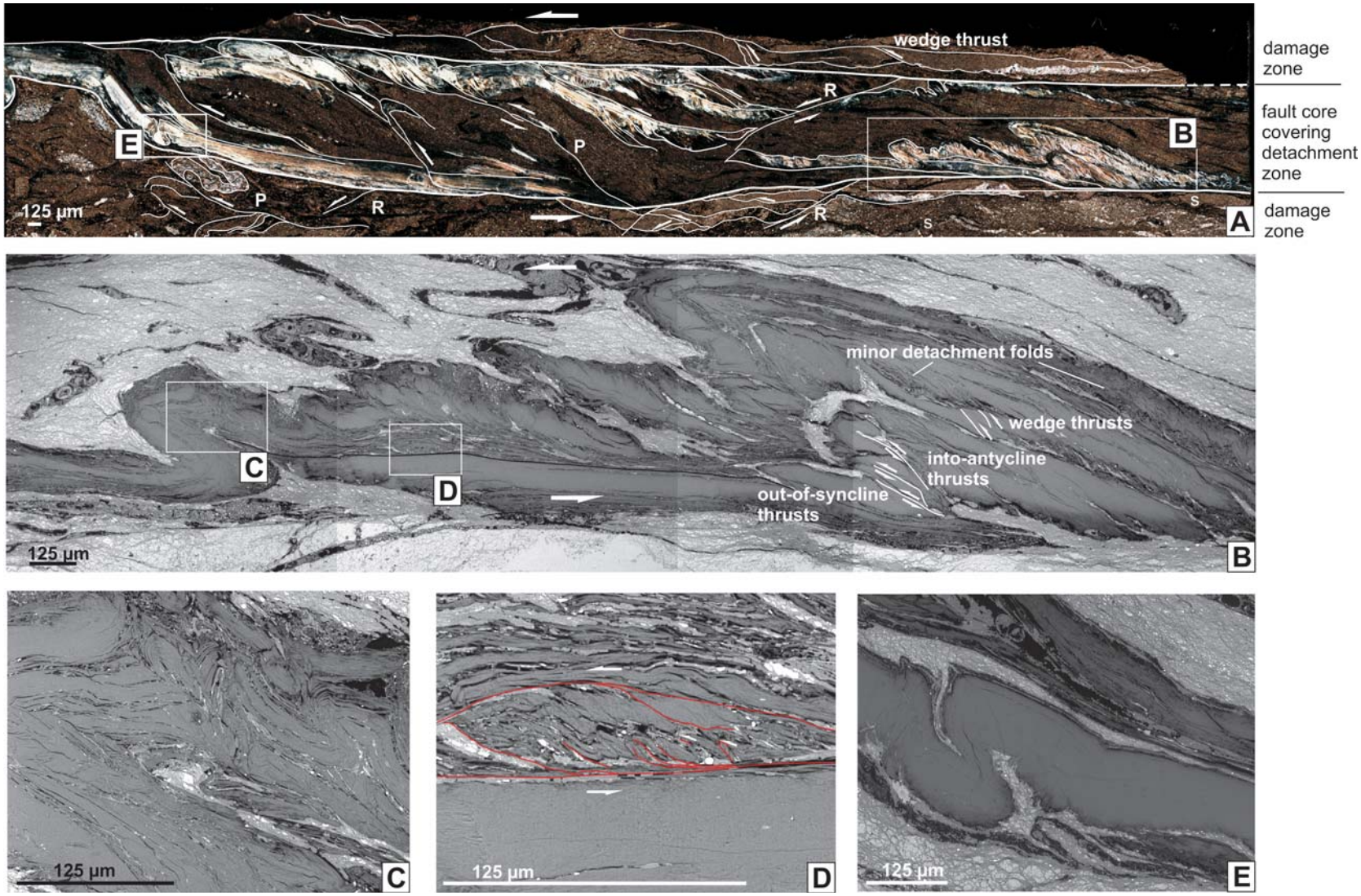

Text-fig. 10. Example of the complex pattern of small-scale folds and faults along the steep thrust fault from the Solinka Stream (sample 3). A – Fault core covering the detachment zone with complex fault-related folds developed along minor thrusts and damage zones covering subsidiary faults and shear fractures, cross-polarised light. B – Asymmetric fold train covering a complex pattern of fault-related folds and fold-accommodation faults (BSE image). C – Internal structure of a box fold (BSE image). D – Internal structure of a minor duplex (BSE image). E – An asymmetric detachment fold related to a ramp (BSE image). Arrows indicate the sense of movement

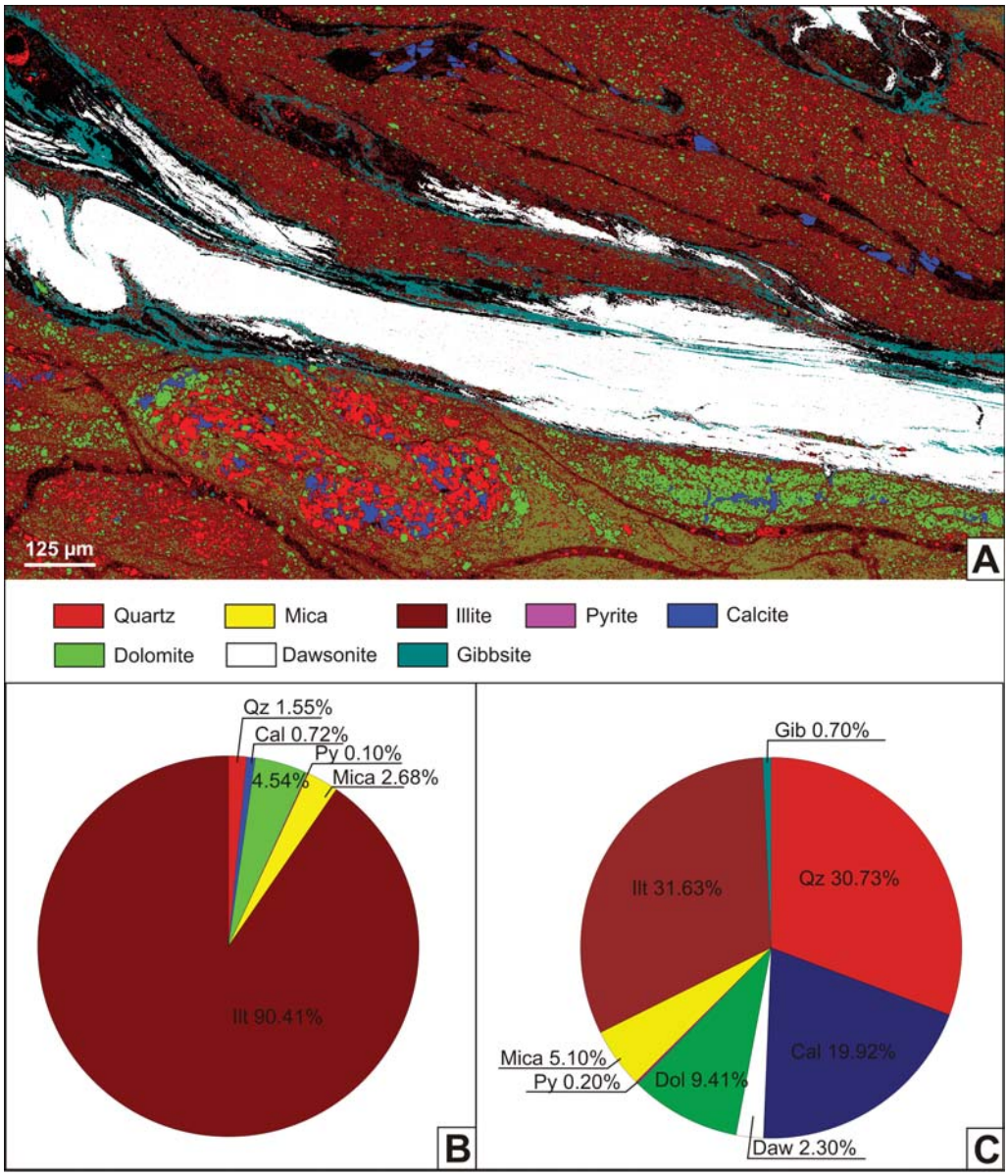

Text-fig. 11. Mineral composition of veins and rocks within a small-scale thrust fault zone, sample 3. A – EDS map covering the core (central and upper part) and the damage zone (lower part). B, C – Percentage diagrams of mineral constituents of rocks within the core and the damage zone respectively

nucleation points for dawsonite weathering. The EDS map shows that gibbsite occurs in close vicinity to the host claystones that are depleted in aluminium and potassium (Text-fig. 9C, D). Simultaneously, gibbsite is absent or scarce within dawsonite veins along the contact with the host claystones that are enriched in aluminium and potassium, which is evidenced by the presence of relatively large mica crystals (Text-fig. 9C, E). A similar relation is observed along thin zones of claystones enriched in fine quartz grains.

Dawsonite associated with carbonate veins shows various arrangements (Text-figs 13A–D, 14A–C) that indicate mutual temporal relationships. Carbonate veins are composite (Text-fig. 15A) or monomineralic, e.g., filled only by calcite (Text-fig. 16A). The former contain the same mineralogical sequence visible within the host rock, showing a distinct zonation of minerals from the outer parts toward the centre, starting with anhedral dolomite, through iron dolomite with well-developed faces, ankerite that forms

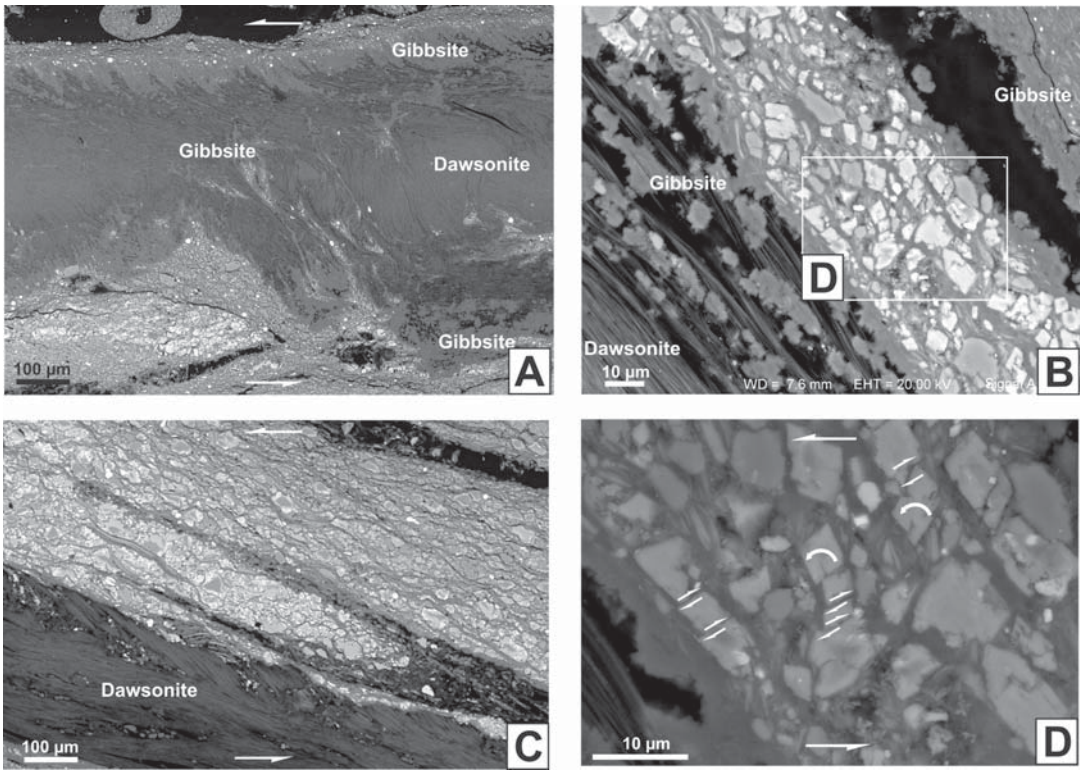

Text-fig. 12. Examples of internal structure of veins and rocks (BSE images). A – Internal fibrous texture of a dawsonite vein with a gibbsite assemblage at the contact with the wall rock and host rock particles within the vein, sample 2. B – Irregular patches of gibbsite distributed within the outer part of the dawsonite vein and within the cataclasite, sample 3. C – Weakly foliated cataclasite with a network of anastomosing shears, sample 3. D – Fracturing, comminution and rotation of grains within a cataclasite sample 3. Arrows indicate the sense of movement

euhedral outgrowths on dolomite faces, and finally anhedral blocky calcite sealing the remaining space of the veins.

Calcite veins are parallel to the fault planes and exceed 1 cm in width. They show diverse fabric. The most common is blocky fabric with grains sub-perpendicular to the vein walls (Text-figs 13B, 14A, B). Some grains, as a result of syntaxial growth show faces pointing towards the centre of the vein (Text-fig. 14B). Elongated calcite is less common (Text-figs 13B, 14A, C). The elongated grains are arranged predominantly slightly oblique to the vein boundary with an inclination of 70–80º (Text-fig. 14C). They show weak preferred orientation. The arrangement of elongated grains parallel to the vein boundary is uncommon and occurs within thin veins separated by shears parallel to the main fault plane (Text-fig. 13B). Both blocky and elongated calcite grains contain host rock inclusions sub-parallel or slightly oblique to the vein boundaries (Text-fig. 13B), which indicate a crack-seal mechanism of vein formation (cf. Ramsay 1980). Additionally, calcite crystals show a progressive increase in size towards the vein centre, pointing to a competition during vein growth (Hilgers and Urai 2002).

Calcite bears evidence of deformation after crystallisation: fracturing (Text-fig. 14B), irregular boundaries suggesting low-temperature grain boundary migration (Text-fig. 14C), and mechanical twinning of type I and II *sensu* Burkhard (1993) (Text-figs 13A, 14A, B). The boundaries of calcite veins are often stylolitic (Text-fig. 15A, B), thus pressure solution and mass transfer within the fault zone played a role in their formation.

Commonly, thin dawsonite veins extend parallel to the fault plane and along previously formed carbonate veins at the boundary of the host rock/calcite veins (Text-figs 13A, 14A, 15A, B, 16A). Dawsonite fibres fill the space along the calcite vein covering its stylolitic morphology (Text-fig. 15A, B), locally splitting into several parallel strands at larger irregularities. They also occur along the fracture network and host rock inclusions within calcite (Text-figs 13B, 14B) and form acicular assemblages that resemble fans or bundles (Text-fig. 14B).

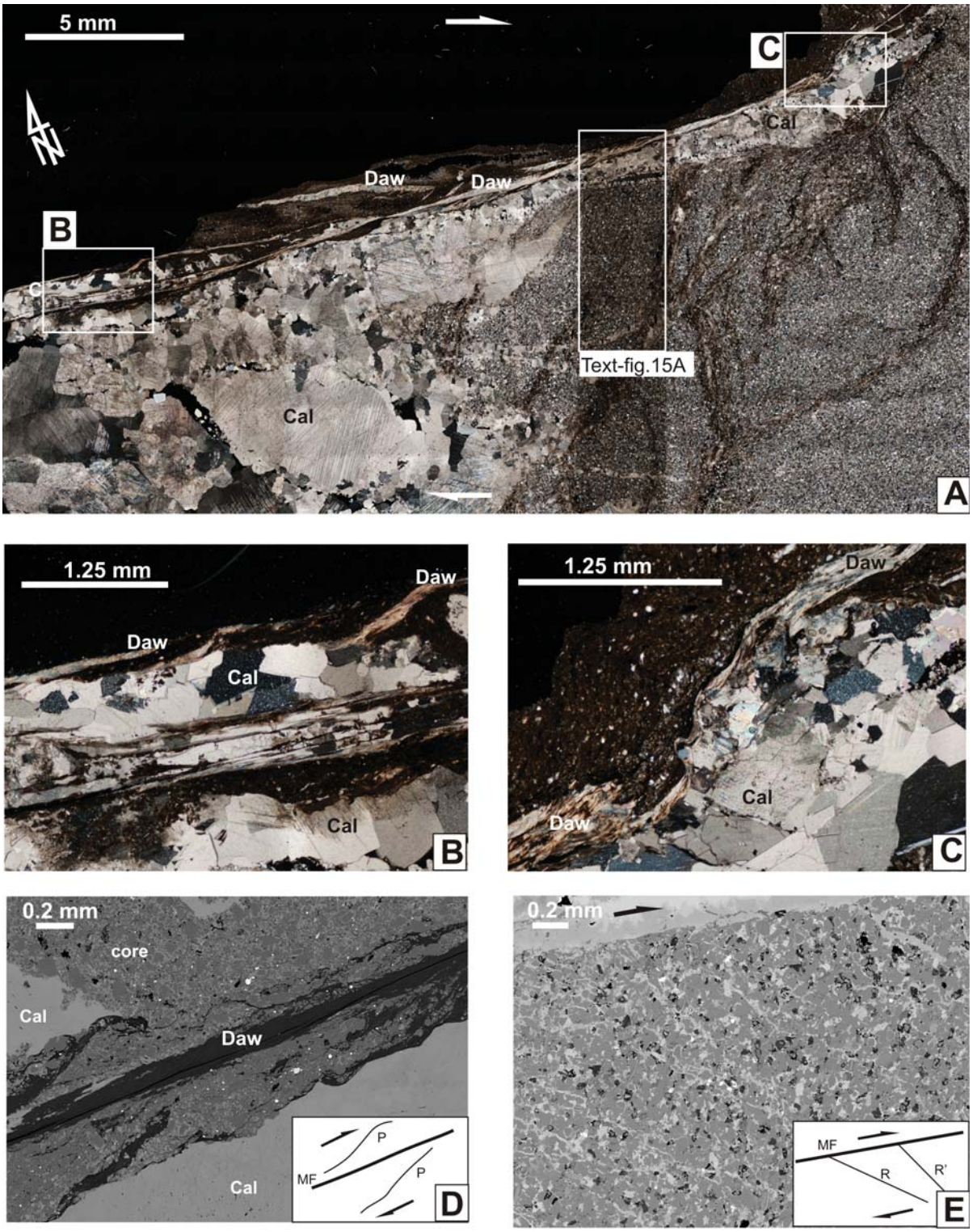

Text-fig. 13. Example of the internal structure of a minor dextral strike-slip fault in the Solinka Stream, sample 7. A – Core with a multi-layered vein of dawsonite lying parallel to a fault-parallel complex carbonate vein and a damage zone developed within calcareous siltstones, cross-polarised light. B – Fragment of a multi-layered calcite vein infilled with blocky and elongated grains, aligned and partly altered by fibrous dawsonite; calcite grains show deformation lamellae (lower-right part), cross-polarised light. C – Fibrous, gently folded dawsonite vein aligned along the stylolitic boundary of a calcite vein, cross-polarised light. D – P shears within the fault core in close vicinity to a calcite vein with a stylolitic morphology (BSE image). E – R and R' shear fracture developed within a damage zone. Arrows indicate the sense of movement

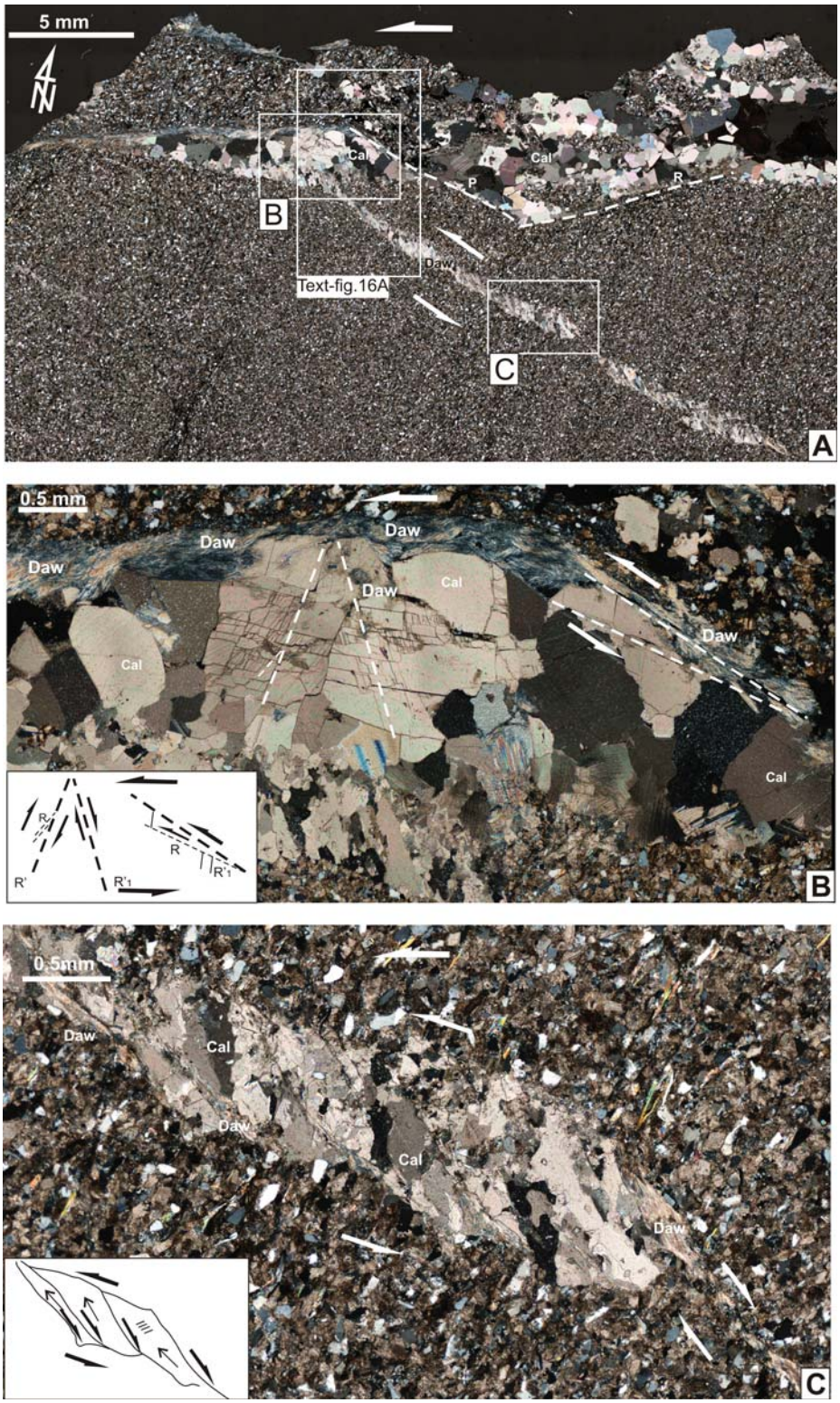

Text-fig. 14. Example of the internal structure of a minor sinistral strike-slip fault from the Solinka Stream, sample 6. A – Network of P-R shears associated with a blocky calcite vein and P shear mineralised by calcite and dawsonite. B – Secondary R' and R'_1 shear fractures developed within calcite, partly aligned by parallel fibrous dawsonite; shear fractures enhance the precipitation of dawsonite arranged in fans and rosettes; calcite grains show deformation lamellae. C – P shear infilled with elongated calcite showing a domino structure developed from antithetic shears infilled with fibrous dawsonite. Cross-polarised light. Arrows indicate the sense of movement

The dawsonite fibres also align elongated calcite grains within subsidiary shear fractures associated with minor faults (Text-fig. 14C). Occasionally, they pass into acicular assemblages between calcite grains or within larger pores of host rocks near the veins. Fault-parallel fibrous and acicular arrangement of dawsonite suggests its syn- and postectonic growth, respectively.

The relationship between calcite and dawsonite within veins, such as dawsonite alignment parallel to previously formed calcite veins, nucleation of dawsonite along host rock inclusions, and fractures within calcite suggests that dawsonite precipitated after calcite within a strike slip-fault zone.

FAULT ZONE MICROSTRUCTURE VERSUS LITHOLOGY

The architecture of minor fault zones is strongly affected by the lithology of the rocks. Commonly, thrust faults show slip localisation subparallel to the bedding planes (Text-figs 9, 10). However, strike-slip faults also break the rocks independently of bedding (Text-figs 13, 14). Macroscopically, the fault cores of thrust and strike-slip faults, if developed, cover the incorporated and deformed incompetent layers of shales (Text-figs 9A–C, 10A, 13A, 15A, B). Some of the strike-slip faults did not develop fault rocks. Instead calcite and/or dawsonite veins formed along them (Text-figs 14A, B, 16A).

Macroscopically, damage zones developed within the relatively more competent mudstones, sandstones, and ankerites. They cover second-order faults and fractures that die out with the increasing distance from the core towards the host rocks. As a consequence, the contact between the fault core and the intact rock represents a gradual transition of decreasing intensity of brittle deformation. This observation implies that competence plays a crucial role in the development of fault zone architecture and deformation of veins. Thus, microstructures within fault zones were characterised in the context of relative competence of the host rock layers (Donath 1970; Ferrill and Morris 2003). Relatively incompetent thin-bedded layers have been observed in all samples and include claystones in relation to the more competent siltstones or mudstones.

It is significant that shaly cores of thrust fault zones have a potential for the development of dawsonite veins (Text-figs 10A, 11A). In turn, the occurrence of dawsonite within subsidiary faults and fractures in damage zones is rare. Exceptions are strike-slip fault zones that display the presence of abundant dawsonite-bearing assemblages along subsidiary faults and fractures, and within pores of the host rocks (Text-figs 14A–C, 15A–D, 16A–C).

Veins and host rocks within fault zones contain microscale structures (Text-figs 9A, 10A–E, 13A–E, 14A–C) that correspond to the sense of movement of the faults recognised during fieldwork. Deformation within the fault zones includes folding, sliding along microfaults, fracturing, and pressure solution. The arrangement and relationship between the microstructures, as well as the mineralogical composition of the host rock and mineral infilling of the microstructures give hints on the multiple deformation history.

Cores of fault zones

The cores of faults in thin sections appear as narrow zones of fault rocks which may be classified as cataclasites (after Sibson 1977; Woodcock and Mort 2008) (Text-figs 12B–D, 13D). Cataclasites comprise predominantly fractured, angular grains with irregular boundaries in a fine and/or clayey matrix. The intensity of grain and mineral fragmentation and deformation differs between the thrust fault zones and strike-slip fault zones.

Cores of thrust fault zones show weak foliation defined by the fault-parallel arrangement of the elongated grains, and/or anastomosing network of shears (Text-fig. 12B–D). Comminution and rotation of grains are common (Text-fig. 12D). Cores of strike-slip fault zones show a fault-oblique arrangement of grains (Text-fig. 13D). BSE images and mineralogical maps show that cataclastic fault rocks slightly differ in composition among individual localities (Text-figs 9D, E, 11B, 15A, E).

The cores cover structural patterns of variable complexity recorded by dawsonite veins related to the faults (Text-figs 9A–C, 10A–E, 13A, D).

Thrust fault zones

The cores of thrust fault zones cover 2.5 mm to 1.8 cm wide detachment zones. The geometry of the detachment zones is defined by a mechanical contrast of the deformed rock and vein sequence. The major detachment thrusts occur most commonly as two separate planes (basal and roof) that limit the detachment zone (Text-fig. 10A). The major detachment thrusts show a straight and flattened geometry that is related to the claystone sequence. Occasionally, stair-step geometry with slip transfer to the upper roof thrust resulted in ramp formation (Text-fig. 10A).

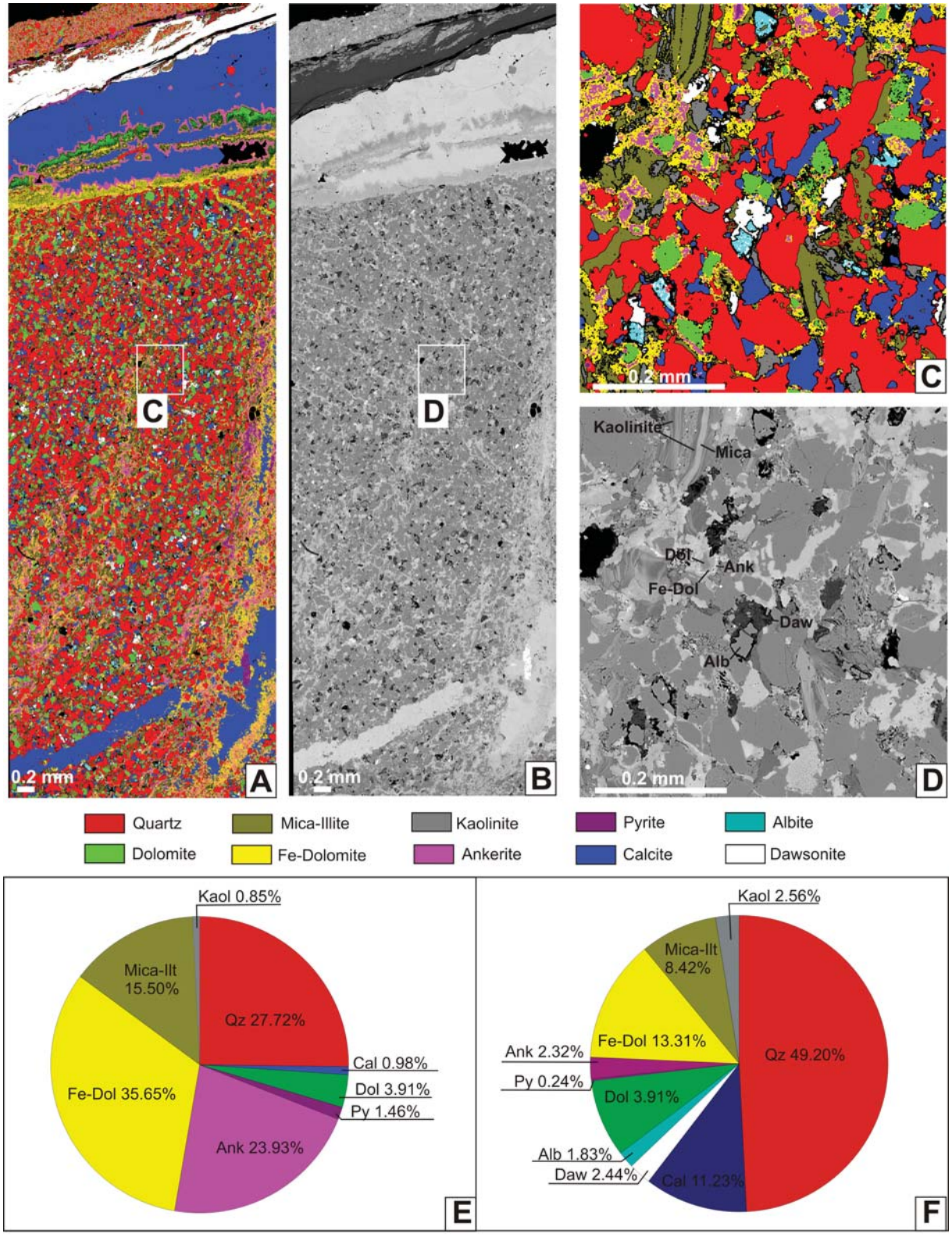

Text-fig. 15. Mineral composition of rocks within the core and the damage zone of a minor dextral strike-slip fault zone, sample 7. A, C – EDS maps. B, D – BSE images. C, D – Fragment of calcareous siltstone covering mineral associations and alteration. E, F – Percentage diagrams of rocks within the core and the damage zone, respectively

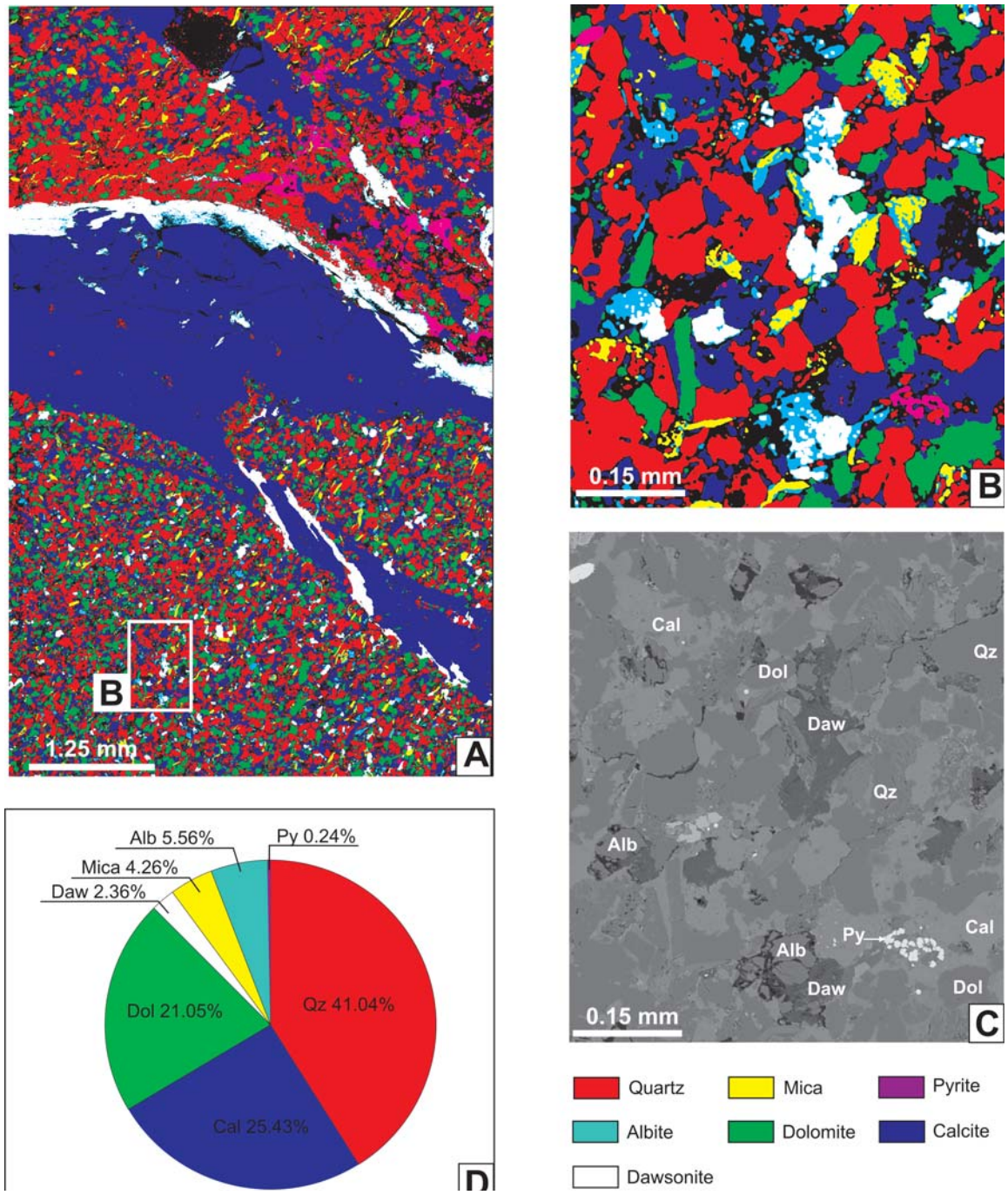

Text-fig. 16. Mineral composition of calcareous siltstone and veins within a minor sinistral strike-slip fault zone, sample 6. A – EDS map. B, C – Fragment of a host rock covering the mineral association and alteration. D – Percentage diagram of the host rock beneath the vein

However, such an interpretation is limited by the scale of observation. Minor detachment thrusts within major detachment zones are multiple, flat, and locally branch into imbricate splays at the leading edge (Text-fig. 10A). The imbricate splays show inclination angles of 35–45º in relation to the detachment horizons. They have listric, sigmoidal to wavy shapes, and occasionally display stylolitic morphology.

Detachment zones also contain second-order normal (Text-fig. 10A) and reversed (Text-figs 9A, 10A)

listric faults synthetic to the detachment thrusts. The latter locally contribute to the imbricate structure formed behind the steep ramp and appear to follow the curvature of that ramp (Text-fig. 10A). The inclination of both types of faults changes across the fault zone from 20º at the roof horizon to 40º at the basal horizon. The geometry and sense of movement of the faults in relation to the major detachments indicate that they represent R and P type faults, respectively (Text-figs 9A, 10A).

The detachment zones host folded dawsonite veins. The small-scale contractional folds include detachment fold trains parallel or oblique to detachment horizons with a continuation into the non-deformed parts of the veins, fault-propagation folds along imbricate splays, secondary faults, and mixed detachment and fault-propagation fold series (Text-figs 10A–E).

Detachment fold trains contain a range of folds from subsequent stages of dawsonite vein deformation (Text-figs 9A–C, 10A–E, 11A, C) represented by folds of various shape profiles from disharmonic folds to box folds (e.g. Mitra 2002, 2003).

Disharmonic fold trains are common (Text-fig. 9A–C). The length of the fold trains reaches a few centimetres. The vergence of the fold trains is generally consistent with the sense of movement of the main thrust. However, the position of individual axial planes varies from tilted towards the sense of movement, through vertical, to an opposite sense of vergence, especially within low-amplitude folds. The folds are predominantly inclined, occasionally upright. They display a full spectrum of inter-limb angles, from gentle to tight, and show variable shapes. The thickness of the veins changes across the disharmonic fold trains with a significant increase within the fold hinges. Thinning of fore-limbs of inclined folds is common. The dawsonite veins form rounded anticlines that are associated with thickening of claystone members within adjacent synclines (cf. Verges *et al.* 2011).

Asymmetric fold trains are located above flat detachment thrusts, locally with the beginning at the leading edge (Text-fig. 10A, B). The folds are tilted toward the sense of fault movement and form short, crowded trains that exceed 1 cm in length. These folds are characterised by steeply to moderately dipping, overturned short forelimbs and moderately dipping back-limbs. The thickness of the veins varies across the fold trains. Anticlines are tight or closed and occasionally show box shapes. The cores of the anticlines and some of the synclines comprise incompetent siltstones, which are deformed and thickened. The folds within the trains show fold accommodation faults represented predominantly by out-of-syncline thrusts (o-s), into-anticline thrusts (i-a) *sensu* Mitra (2002) within the hinges, and limb wedge thrusts (l-w) (Text-fig. 10B). Dawsonite veins split into a series of fibres that were deformed individually and resulted in a thickness increase within limbs and/or fold hinges. The individual dawsonite fibres within the hinges of box folds are cracked, displaced and secondarily folded along the minor thrusts (Text-fig. 10B, C). The axial planes of these minor folds form a flower structure showing a consistent, as well as an opposite sense of vergence in relation to the major box fold (Text-fig. 10B, C). Limbs of anticlines within fold trains show also second-order detachment folds formed along individual fibres or aggregates of fibres (Text-fig. 10B).

Some of the minor detachment folds show a highly complex geometry (Text-fig.10B, C) with a subdivision into upper and inner layers (Text-fig. 10D). The upper layers are deformed into asymmetric high-relief detachment folds that in a more mature stage evolved into high-relief fault-propagation folds (Text-fig. 10D). Fault-propagation folds show steeper and narrower reduced fore-limbs in relation to their back-limbs. The inner layers of minor detachment folds show little internal deformation expressed by low amplitude harmonic buckle folds (Text-fig. 10D). Locally, the back-limbs of the folds evolved along flat ramps into fault-bend low-amplitude anticlines. They are transported by the lower order detachment above the low-relief trains of asymmetric detachment folds partly imbricated along into-anticline thrusts into a series of fault-propagation folds (e.g., Boyer and Elliot 1982; Mitra 1986) that partly evolved in a more mature stage into breakthrough fault-propagation folds (Text-fig. 10D). These folds are very tight, almost isoclinal, with cracked hinges. Fault-propagation folding within the train is minor, and is considered to be a secondary process that evolved from earlier detachment folding (e.g., Dixon and Liu 1992).

Breakthrough fault-propagation folds (after Suppe and Medwedeff 1990) occur in series within the detachment zones (Text-fig. 10A) and contribute to low-relief imbricated structures. Individual slices associated with P thrust faults consist of synclinal breakthrough, tight fault-propagation folds with thinned and locally partly reduced steep forelimbs, rounded or acute hinges, and moderately to gently dipping back-limbs. The breakthrough fault-propagation folds developed in close vicinity of the roof detachment, in the hinterland of the thinnest part of the detachment zone. Slip along the thrust faults is

hardly possible to estimate, because of the dense network of thrust faults within the sets. The formation of breakthrough fault-propagation folds is closely related to the stair-stepping geometry of the basal major detachment and formation of a ramp that enhanced contraction within the detachment zone.

Strike-slip fault zones

The cores of strike-slip faults are covered with multi-layered dawsonite veins, often associated with carbonate veins parallel to the main fault (Text-figs 13A–D, 15A, B).

Dawsonite veins that align calcite veins are rather continuous, locally slightly folded. Individual low-amplitude folds or trains of folds are located within wider parts of the cores in close vicinity to irregularities in previous calcite veins (Text-figs 13A–C, 15A, B). The folds are asymmetric and show a vergence with the same sense of movement as that of the sampled fault. The inter-limb angles vary from gentle to tight (Text-fig. 13A–C).

Locally, dawsonite veins show strands oriented slightly oblique to the fault plane (Text-fig. 13A). The inclination of strands tends to change across the core from c. 15º at the beginning to almost 0º within the core. The strands occur individually or align to the previously formed multi-layered calcite veins at their boundaries. Some of the dawsonite fibres at the end of strands continue into calcite crystals. Individual veins within the core bear traces of shortening related to continuous fault movement.

Damage zones

Damage zones of thrust faults and strike-slip faults host subsidiary structures but they differ in form and distribution in relation to the host rock composition (Text-figs 11 A, C, 15A, C, D, F, 16A–D).

Damage zones in the vicinity of detachment zones host minor fold-accommodation faults represented by thrust wedges and subsidiary microfaults (Text-fig. 10A). Minor thrust wedges occur in the hanging and footwalls (Text-fig. 10A). They are synthetic to the sense of movement along the detachment horizons. Traces of thrust wedges are bent or wavy in shape. Displacement of competent layer fragments along thrust wedges caused local thickening and buckling of the layers.

Subsidiary microfaults occur within footwalls and initiate at the basal detachment thrust. They continue through overlying rock layers that are defined by increased competence, and die out at the boundary of contrasting competence layers or within layers with higher competence (Text-fig. 10A). Fault traces within claystones are bent or wavy in shape, and overprinted by stylolitic seams (Text-fig. 10A). They occur in two synthetic sets that show opposite inclinations of c. 15–20º. Occasionally they form weakly developed meshes (Text-fig. 10A). The spacing between the faults within particular sets ranges from a few millimetres to 1 cm. They represent R- and P-type faults, respectively. Faults of types R and P are closed, aligned by phyllosilicates.

The structure of strike-slip fault damage zones is related to the composition of host rocks represented by calcareous siltstones with carbonate cements. The pore cement contains the following sequence of carbonate minerals: i) dolomite–iron-rich dolomite–ankerite–calcite–dawsonite (Text-fig. 15A–D, F) ii) calcite and dawsonite (Text-fig. 16A–D). Dolomite is corroded, locally cracked and overgrown by euhedral iron-rich dolomite. Both of the dolomites show overgrowths and internal anhedral assemblages of ankerite. The porosity of the rocks is sealed by calcite and dawsonite.

Layers of more competent calcareous siltstones host subsidiary shear fractures of variable distribution, size, and mineral infilling related to host rock cement (Text-figs 13A, E; 14A–C, 15A, B, 16A).

In thin section a dense system of thin R and R' shear fractures pervasively cuts the host calcareous siltstones within the damage zone. Spacing between shear fractures reaches 0.5 mm. The shear fractures crosscut some of the host rock grains or bypass them, which results in irregular traces. The fractures are sealed predominantly with iron-rich dolomite that is partially corroded and secondarily infilled with ankerite and rarely with calcite (Text-fig. 15A, C).

R_1' shear fractures cut the R and R' system and show wider and less regular distribution in relation to the R and R' system. R_1' shear fractures are aligned by parallel elongated grains of mica (Text-fig. 15A, F). They are inclined at an angle of c. 60–70º to the sampled fault. R_1' shear fractures are infilled with carbonate minerals in a similar sequence as the fault-parallel veins and host rocks, i.e. dolomite, iron-rich dolomite, ankerite, and calcite.

Siltstones also host subsidiary microfaults developed in one synthetic set with an inclination of individual members at 25–35º in relation to the sampled fault (Text-figs 14A, 16A). Kinematically and geometrically they correspond to P shears. The spacing of the microfaults changes across the damage zone from a few to several centimetres. The segmentation of microfaults resulted in the formation of dilational

veins infilled with calcite. The veins show blurry boundaries because they have the same composition as the host rock cements. Calcite grains are slightly oblique to the vein boundaries. The inclination of grains towards the sense of movement of the shear fracture indicate its syntectonic growth. Dawsonite fibres occupy antithetic shears that bound dilational veins and probably alter calcite crystals within the veins.

DISCUSSION

The structural pattern developed within the fault zones of the Fore-Dukla Thrust Sheet contains evidence for the upper crustal deformation of Palaeogene flysch deposits. The fault zone architecture combined with the succession of mineral infilling provides evidence for dawsonite formation along progressively developed structures within the thrust fault and the strike-slip fault zones, and after deformation continuing until recently.

Thrust fault zones yield evidence for subsequent deformation resulting from the accommodation of continuous shortening within detachment zones by: 1. frictional granular flow of rocks resulting in cataclasis, 2. formation of bedding and detachment-parallel dawsonite veins, and 3. detachment-induced folding and faulting of veins evidenced by the sequence of disharmonic and fault-related folds (Text-figs 9A–C, 10A–E, 11A). Damage zones record deformation by the formation of thrust wedges within the hanging walls and a network of R and P shear fractures within the footwalls. The constraint of fibrous dawsonite veins to bedding planes of shales and detachment zones within thrust fault zones indicates that these structures were permeable during thrusting.

The strike-slip fault zones yield evidence for deformational phases recorded by: 1. formation of fault parallel veins infilled with a sequence of dolomite–iron-rich dolomite–ankerite–calcite, followed by 2. formation of fault-parallel dawsonite veins that have been locally folded during progressive displacement along the fault (Text-figs 13A, 14A). Commonly, the geometry of previous carbonate veins defines the extent and deformation of dawsonite veins along strike-slip faults. Formation of veins along the faults was accompanied by simultaneous sealing of subsidiary shear fractures within damage zones and host rock porosity. The process likely resulted in progressive cementation and decrease of fault zone permeability (cf. Gratier and Gueydan 2007).

Structural pattern versus lithology

Thrust and strike-slip fault zones generally show evidence of brittle faulting processes (cf. Mastella 1988; Konon 2000; Rybak-Ostrowska *et al.* 2017). However, layers of different grain size and mineralogical composition reveal different styles of deformation. Claystones from the Menilite Beds are dominantly deformed by cataclastic flow within fault cores and fault-related folding within detachment zones (Text-figs 9A–C, 10A–F). Siltstones from the Menilite Beds contribute to the damage zones (Text-fig. 10A) and along with sandstone layers they show subsidiary shear fractures. The fault cores and damage zones show evidence for pressure solution. Conversely, the thrust fault zones within the Menilite Beds lack widely distributed dilational jogs or other extensional structures sealed by dawsonite or calcite.

The calcareous siltstones of the Transition Beds are more prone to fracturing and show composite mineral veins along the main fault plane as well as a dense system of subsidiary shear fractures infilled with dolomite–iron-rich dolomite–ankerite–calcite (Text-fig. 15A), or calcite and dawsonite (Text-fig. 16A). The latter assemblage occurs only within damage zones of strike-slip fault zones. The evidence of pressure solution is predominantly recorded within the mineral infilling, only occasionally within the host rocks.

In summary, the formation of structures depends on the mineral composition of the host rocks: very fine-grained rocks with predominant phyllosilicate constituents such as claystones enhance cataclastic deformation, comminution of grains and development of foliation. These rocks have low permeability and produce a sealing system. Thus fluid pathways are limited to faults and bedding planes. Conversely, fine-grained rocks with a quartz grain-supported matrix such as calcareous siltstones enhance fracturing and the development of extensional structures within fault zones, having potential for fluid flow. Additionally, the porosity of these rocks may contribute to the formation of a complex permeability system.

Dawsonite veins formation

The relationship of the mineralogical composition of syntectonic veins and host rocks (Text-figs 9, 11, 15, 16) gives some hints on fluid flow within fault zones and related fluid/rock interactions. For example, syntectonic fibrous dawsonite veins in thrust fault zones are closely related to claystones (Text-figs 9A–D,

10A, 11A, B, 15A, C). However, the clay matrix lacks albite, which is supposed to be the potential source of sodium for dawsonite formation (e.g., Baker *et al.* 1995; Moor *et al.* 2005, Worden 2006). This relationship suggests that sodium for dawsonite formation could have been provided from fluids infiltrating the thrust fault zones. Previous studies on natural and synthesized dawsonite (Moor *et al.* 2005; Worden 2006; Bénézeth *et al.* 2007) followed by numerical modelling (Hellawang *et al.* 2011; Trémosa *et al.* 2014) indicate that dawsonite precipitates from acidic CO_2-rich fluids. The fluids may enhance alteration of the rock constituents, including dissolution of aluminosilicates (e.g., clay minerals, cf. Johnson *et al.* 2004; Bénézeth *et al.* 2007; Hellawang *et al.* 2011; Trémosa *et al.* 2014) resulting in the liberation of aluminium. A similar process might have affected the clay matrix in the Menilite Beds and resulted in the syntectonic growth of fibrous dawsonite. Consequently, gibbsite occurring in the outer parts of dawsonite veins might have formed by the decomposition of dawsonite (cf. Palayangoda and Nguyen 2015), probably related to post-thrusting processes combined with fluid flow within thrust fault zones. This possibility would explain the irregular distribution of gibbsite assemblages within fibrous dawsonite veins (Text-fig. 12A, B). However, this complex hypothesis needs further geochemical analyses.

The process of fluid migration within strike-slip fault zones dissecting the Transition Beds is recorded by fault-related veins and host rock carbonate cements composed of a dolomite–iron-rich dolomite–ankerite–calcite sequence. Authigenic precipitation of dolomite is considered to take place at shallow burial during early diagenesis within the upper Eocene–Oligocene rocks of the Outer Carpathians (Narębski 1957; Rajchel and Szczepańska 1997; Szczepańska 2003). However, the sequence of dolomite–iron-rich dolomite–ankerite cements within the Menilite and Krosno Beds studied in the Dukla Nappe (Bojanowski 2014) indicates subsequent burial of rocks from shallow depths towards the decarboxylation zone. Considering the mineral succession within the fault-parallel veins and subsidiary shear fractures within the strike-slip fault zones, it is plausible that the dolomite–ankerite–calcite precipitation sequence was associated with the strike-slip faulting. It is also possible that the maintained porosity was capable of fluid channelling during the faulting (Text-fig. 15A, B). Syntectonic dawsonite formation followed the subsequent strike-slip faulting localised along the earlier carbonate veins partitioned by pressure solution along fault surfaces (Text-fig. 15A, B).

Dawsonite veins from the strike-slip fault zone within the Transition Beds lack a gibbsite-bearing assemblage. This fact can be explained by the presence and dissolution of albite within the host rocks (Text-figs 15C, D, 16B, C). Successive replacement of albite by dawsonite is recorded by relics of albite grains within dawsonite that infilled the pores of host rocks. This observation implies that the host rocks were porous and permeable and as a result were infiltrated by fluids. Successive chemical dissolution of albite has been probably enhanced by mechanical disintegration related to faulting. This process might have provided a constant source of sodium for dawsonite formation (cf. Baker *et al.* 1995; Hutcheon *et al.* 2016).

The beginning of dawsonite formation within the Fore-Dukla Thrust Sheet in fault zones coincides with the maturation of the low permeable organic-rich Menilite Beds followed by generation and expulsion of hydrocarbons, which took place during Miocene overthrusting (Kotarba and Koltun 2006). However reducing hydrocarbon-rich fluids contain minimum CO_2 (e.g. Hurai *et al.* 2006). Thus the occurrence of dawsonite limited to fault zones cutting the Menilite Beds and the stratigraphically younger Transition Beds suggests the influx of CO_2-rich fluids from deep-seated units (c.f. Hurai *et al.* 2015).

Fluid pathways in this setting were defined by the distribution of low permeable shales and the fault zone architecture. Distribution of dawsonite within thrust fault zones dissecting the Menilite Beds suggests that thrusts and bedding planes might have been one of the main pathways for fluid migration within generally low permeable shales.

Burial and diagenesis of sediments during continuous deformation caused their cementation and porosity reduction within permeable siltstones. All these processes enhanced fluid flow through faults (e.g. Moore and Vrolijk 1992; Nemčok *et al.* 2009, Faulkner *et al.* 2010), although additional pathways for fluid migration could have been provided by porous siltstones. Based on the results of fluid inclusion study in calcite and quartz in the OCFTB (Młynarczyk 1996; Jarmołowicz-Szulc and Dudok 2005; Hurai *et al.* 2006; Jarmołowicz-Szulc 2009; Jarmołowicz-Szulc *et al.* 2012), we suggest that precipitation of carbonate minerals within strike-slip fault zones could have been linked with the successive migration of CO_2-rich fluids through the fault zones.

The present-day precipitation of dawsonite as well as the formation of tufa covers on rocks within the fault zones indicate a constant migration and con-

tinuing influence of CO_2-rich fluids within the Fore-Dukla Thrust Sheet.

Further research is necessary to establish the isotopic composition of dawsonite and other carbonate minerals along with tufa deposits within the fault zones. Comparison of the oxygen and carbon isotope compositions should allow for deciphering the source of CO_2 during and after the activity of the fault zones in the Fore-Dukla Thrust Sheet. Additionally, chemical analysis of seeping waters within the fault zones should provide data on the present day processes operating within fault zones.

CONCLUSIONS

The structural pattern of fault zones contains evidence for upper crustal deformation. Fault zones covered with dawsonite record the following successive development of structures within the Fore-Dukla Thrust Sheet: i) detachment and folding by buckling controlled by movement along thrust faults; ii) faulting associated with the shortening and resulting in subsequent fault propagation folding, breakthrough thrust faulting, and imbrications; and iii) strike-slip faulting.

The microstructural patterns along with the relative sequence of carbonate mineral growth within the fault zones indicate subsequent fluid flow. Fluid pathways in this setting were defined by the distribution of low permeable rocks and the fault zone architecture. Thus fluid pathways within low permeable incompetent rocks, such as shales from the Menilite Beds were limited predominantly to bedding planes and thrust faults. Moreover, fluid pathways within more permeable and competent rocks such as siltstones or ankerite of the Menilite and Transition beds, were also provided by a subsidiary fault and fracture network within damage zones.

The architecture of the fault zones combined with syntectonic dawsonite precipitation provide evidence for the formation of dawsonite along progressively developed structures within thrust fault zones and strike-slip fault zones.

The thrust fault zones within the Menilite Beds dominated by claystones are mineralised mainly by dawsonite and superimposed gibbsite. In contrast, the strike-slip fault zones within the Transition Beds show a complex sequence of sealing minerals, from dolomite followed by iron-rich dolomite, ankerite, calcite, to late dawsonite. Contemporaneous precipitation of dawsonite within fault zones suggests an ongoing process of the formation of dawsonite.

Acknowledgements

This project was supported by the Faculty of Geology, University of Warsaw (BST 160600/2, 163702) and European Regional Development Fund (POIG.02.02.00-00-025/09). We would like to thank Vratislav Hurai and Stanisław Mazur for constructive comments that significantly improved the manuscript. We would also like to thank Andrzej Konon for discussions on the early version of the manuscript and Michał Wyglądała for assistance during fieldwork.

REFERENCES:

Andreucci, B., Castelluccio, A., Jankowski, L., Mazzoli, S., Szaniawski, R. and Zattin, M. 2013. Burial and exhumation history of the Polish Outer Carpathians: Discriminating the role of thrusting and post-thrusting extension. *Tectonophysics*, **608**, 866–883.

Arndt, M., Virgo, S., Cox, S.F. and Urai, J.L. 2014. Changes in fluid pathways in calcite vein mesh (Natih Formation, Oman Mountains): insights from stable isotopes. *Geofluids*, **14**, 391–418.

Baker, J.C., Bai, G.P., Hamilton, P.J., Golding, S.D. and Kenee, J.B. 1995. Continental-scale magmatic carbon dioxide seepage recorded by Dawsonite in the Bowen-Gunnedah-Sydney basin system, Eastern Australia. *Journal of Sedimentary Research*, **A65**, 522–530.

Bénézeth, P., Palmer, D.A., Anovitz, M.L. and Horita, J. 2007. Dawsonite synthesis and reevaluation of its thermodynamic properties from solubility measurements: Implications for mineral trapping of CO_2. *Geochimica et Cosmochimica Acta*, **71**, 4438–4455.

Bojanowski, M.J. 2007. The onset of orogenic activity recorded in the Krosno shales from Grybów unit (Polish Outer Carpathians). *Acta Geologica Polonica*, **57**, 509–522.

Bojanowski, M.J. 2014. Authigenic dolomites in the Eocene–Oligocene organic carbon-rich shales from the Polish Outer Carpathians: evidence of past gas production and possible gas hydrate formation in the Silesian basin. *Marine and Petroleum Geology*, **51**, 117–135.

Boyer, S.E. and Elliot, D. 1982. Thrust Systems. *American Association Petroleum Geologists Bulletin*, **66**, 1196–1230.

Burchfiel, B.C. and Royden, L. 1982. Carpathian foreland fold and thrust belt and its relation to Pannonian and other basins. *The American Association of Petroleum Geologists Bulletin*, **66**, 241–256.

Burkhard, M. 1993. Calcite twins, their geometry, appearance and significance as stress-strain markers and indicators of tectonic regime: a review. *Journal of Structural Geology*, **15**, 351–368.

Caine, J.S., Evans, J.P. and Forster, C.B. 1996. Fault zone architecture and permeability structure. *Geology*, **24**, 1025–1028.

Chester, F.M., Evans, J.P. and Biegel, R.L. 1993. Internal structure and weakening mechanism of the S.Andreas Fault. *Journal of Geophysical Research*, **98**, 771–786.

Chester, J.S. 1996. Geometry and kinematics of a passive-roof duplex in the interior of the Idaho-Wyoming-northern Utah thrust belt. *Bulletin of Canadian Petroleum Geology*, **44**, 363–374.

Chester, J.S. 2003. Mechanical stratigraphy and fault-fold interaction, Absaroka thrust sheet, Salt River Range, Wyoming. *Journal of Structural Geology*, **25**, 1171–1192.

Csontos, L., Nagymarosy, L., Horvath, F. and Kováč, M. 1992. Tertiary evolution of the Intra-Carpathian area: a model. *Tectonophysics*, **208**, 221–241.

Dahlstorm, C.D.A. 1969. The upper detachment in concentric folding. *Canadian Petroleum Geologists Bulletin*, **17**, 326–346.

Dahlstorm, C.D.A. 1990. Geometric constraints derived from the law of conservation of volume and applied to evolutionary models for detachment folding. *American Association of Petroleum Geologists Bulletin*, **74**, 336–344.

Dixon, J.M., and Liu, S. 1992. Centrifuge modelling of the propagation of thrust faults. In: McClay, K.R. (Ed.), Thrust Tectonics, pp. 53–70. Chapman & Hall; London.

Donath, F.A. 1964. Strength variation and deformational behaviour of anisotropic rocks. In: Judd, W.R. (Ed.), State of stress in the Earth's crust, pp. 281–298. New York; Elsevier.

Eichhubl, P. and Boles, J.R. 2000. Focused fluid flow along faults in the Monterey Formation, coastal California. *Geological Society of America Bulletin*, **112**, 1667–1679.

Erickson, S.G. 1996. Influence of mechanical stratigraphy on folding vs. faulting. *Journal of Structural Geology*, **18**, 443–450.

Estublier, A., Fornel, A., Brosse, É., Houel, P., Lecomte, J.C., Delmas, J. and Vincké, O. 2017. Simulation of a Potential CO_2 Storage in the West Paris Basin: Site Characterization and Assessment of the Long-Term Hydrodynamical and Geochemical Impacts Induced by the CO_2 Injection. *Oil & Gas Science and Technology – Revue IFP Energies nouvelles*, **72**, 1–24.

Faulkner, D.R., Jackson, C.A.L., Lunn, R.J., Schlische, R.W., Shipton, Z.K., Wibberley, C.A.J. and Withjack, M.O. 2010. A review of recent developments concerning the structure mechanics and fluid flow properties of fault zones. *Journal of Structural Geology*, **32**, 1557–1575.

Ferrill, D.A. and Morris, P. 2008. Fault zone deformation controlled by carbonate mechanical stratigraphy, Balcones fault system, Texas. *American Association of Petroleum Geologists Bulletin*, **92**, 359–380.

Ferrini, V., Martarelli, L., De Vito, C., Cina, A. and Deda, T. 2003. The Koman dawsonite and realgar-orpiment deposit, northern Albania; inferences on processes of formation. *Canadian Mineralogist*, **41**, 413–427.

Fischer M.P. and Jackson, P.B. 1999. Stratigraphic controls on deformation patterns in fault-related folds: a detachment fold example from the Sierra Madre Oriental foreland, northeast Mexico. *Journal of Structural Geology*, **21**, 613–633.

Fodor, L., Csontos, L., Bada G., Gyorfi, I. and Benkovics, L. 1999. Tertiary tectonic evolution of the Pannonian Basin system and neighbouring orogens: a new synthesis of paleostress data. In: Durand, B., Jolivet L., Horvath, F., Seranne M. (Eds), The Mediterranean Basins: Tertiary extension within the Alpine Orogen. *Geological Society, London, Special Publications*, **156**, 295–334.

Gągała, Ł., Vergés, J., Saura, E., Malata, T., Ringenbach, J.-C., Werner, P. and Krzywiec, P. 2012. Architecture and orogenic evolution of the northeastern Outer Carpathians from cross-section balancing and forward modeling. *Tectonophysics*, **532**, 223–241.

Golab, A.N., Carr, P.F. and Palamara, D.R. 2006. Influence of localised igneous activity on cleat dawsonite formation in Late Permian coal measures, Upper Hunter Valley, Australia. *International Journal of Coal Geology*, **66**, 296–304.

Gratier, J.-P. and Gueydan, F. 2007. Deformation in the Presence of Fluids and Mineral Reactions. Effect of Fracturing and Fluid-Rock Interaction on Seismic Cycles. In: Handy, M., Hirth, G., Rice, J., Hovius, N. and Friedrich, A. (Eds), The Dynamics of Fault Zones (95th Dahlem Conference), pp. 319–356. MIT Press; Cambridge, MA.

Gucik, S. and Wójcik, A. 1982. Explanation to the Geological Map of Poland, Przemyśl-Kalników sheet, scale 1:200000. Wydawnictwa Geologiczne; Warszawa.

Guterch, A., Grad, M., Keller, G.R., Posgay, K., Vosar, J., Spicak, A., Brueckel, E., Haynal, Z., Thybo, H. and Selvi, O. 2000. The Celebration 2000 Seismic Experiment. Joint Meeting of EURO-PROBE (TESZ) and PACE Projects. Zakopane/ Holy Cross Mountains, Poland. Abstracts volume, pp. 29–32. Warszawa.

Haczewski, G., Bąk, K., Kukulak, J., Mastella, L. and Rubinkiewicz, J. 2000. Explanation to the Geological Map of Poland, Ustrzyki Górne sheet, scale 1:50000. Polish Geological Institute Archive; Warszawa.

Hayes, M. and Hanks, C.L. 2008. Evolving mechanical stratigraphy during detachment folding. *Journal of Structural Geology*, **30**, 548–564.

Hellawang, H., Declercq, J. and Aagaard P. 2011. Why is Dawsonite Absent in CO_2 Charged Reservoirs? *Oil and Gas Science Technology – Revue IFP Energies nouvelles*, **66**, 119–135.

Hilgers, C. and Urai, J. 2002. Microstructural observations on natural syntectonic fibrous veins: implications for the growth process. *Tectonophysics*, **352**, 257–274.

Hurai, V., Huraiová, M., Slobodnik, M. and Rainer, T. 2015. Geofluids: Developments in Microthermometry, Spectroscopy, Thermodynamics, and Stable Isotopes, 162 p. Elsevier; Amsterdam.

Hurai, V., Marko F., Tokarski, A.K., Świerczewska A., Kotulová, J. and Biroň, A., 2006. Fluids inclusion evidence for deep burial of the Tertiary accretionary wedge of the Carpathians. *Terra Nova*, **18**, 440–446.

Hutcheon, I., Shevalier, M., Durocher, K., Bloch, J., Johnson, G., Nightingale, M., and Mayer, B. 2016. Interactions of CO_2 with formation waters, oil and minerals and CO_2 storage at the Weyburn IEA EOR site, Saskatchewan, Canada. *International Journal of Greenhouse Gas Control*, **53**, 354–370.

Jamison, W.R. 1987. Geometric analysis of fold development in overthrust terranes. *Journal of Structural Geology*, **9**, 207–219.

Jankowski, L., Kopciowski, R., Ryłko, W., Danysh, V., Tsarnenko, P., Janoćko, J. and Jacko, S. 2004. Geological Map of the Outher Carpathians: Borderlands of Ukraine, Poland and Slovakia, 1:200 000. Państwowy Instytu Geologiczny; Warszawa.

Jarmołowicz-Szulc, K. 2009. Recent contribution to mineralogical and geochemical studies in the Carpathians. *Mineralogical Review*, **59**, 42–55.

Jarmołowicz-Szulc, K. and Dudok, I. 2005. Migration of palaeofluids in the contact zone between the Dukla and Silesian units, Western Carpathians – evidence from fluid inclusions and stable isotopes in quartz and calcite. *Geological Quarterly*, **49**, 291–304.

Jarmołowicz-Szulc, K., Karwowski, Ł. and Marynowski, L. 2012. Fluid circulation and formation of minerals and bitumens in the sedimentary rocks of the Outer Carpathians – Based on studies on the quartz-calcite-organic matter association. *Marine and Petroleum Geology*, **32**, 138–158.

Johnson, J.W., Nitao, J.J., Steefal, C.I. and Knauss, K.G. 2004. Reactive transport modelling of CO_2 storage in saline aquifers to elucide fundamental processes, trapping mechanism and sequestration partitioning. In: Baines, S.J. and Worden, R.H. (Eds), Geological Storage of Carbon Dioxide. *Geological Society, London, Special Publications*, **233**, 107–128.

Jucha, S. and Kotlarczyk, J. 1961. Seria menilitowo-krośnieńska w Karpatach fliszowych. *Prace Geologiczne PAN*, **4**, 1–115.

Kamilli, R.J. and Ohmoto, H. 1977. Paragenesis, Zoning, Fluid Inclusion, and Isotopic Studies of the Finlandia Vein, Colqui District, Central Peru. *Economic Geology*, **72**, 950–982.

Kharaka, Y., Cole, D.R., Hovorka, S.D., Gunter, W.D., Knauss, K.G. and Freifeld, B.M. 2006. Gas-water-rock interactions in Frio formation following CO_2 injection: implications for the storage of greenhouse gases in sedimentary basins. *Geology*, **34**, 577–580.

Kiràly, C., Szamosfalvi, Á., Zilali-Sebess, L., Kónya, P., Kovács, I.J., Sendula, E., Szabó, C. and Falus, G. 2016. Caprock analysis from the Mihályi-Répcelak natural CO_2 occurrence, Western Hungary. *Environmental Earth Sciences*, **75**, [635] doi.org/10.1007/s12665-016-5399-6.

Knauss, G.K., Johnson, J.W. and Steefel, C.I 2005. Evaluation of the impact of CO_2, co-contaminant gas, aqueous fluid and reservoir rock interactions on the geologic sequestration of CO_2. *Chemical Geology*, **217**, 339–350.

Knipe, J.P. 1993. The influence of fault zone processes and diagenesis on fluid flow. In: Horbury, A.D. and Robinson, A. (Eds), Diagenesis and Basin Development. *American Association of Petroleum Geologists Studies in Geology*, **36**, 135–151.

Konon, A. 2000. Deformation mechanism of cataclastic rocks from fault zones in the Beskid Wyspowy Mountains (Poland). *Acta Geologica Polonica*, **50**, 387–392.

Konon, A. 2001. Tectonics of the Beskid Wyspowy Mountains (Outer Carpathians, Poland). *Geological Quarterly*, **45**, 179–204.

Köster, J., Kotarba, M., Lafargue, E. and Kosakowski, P. 1998. Biomarker geochemistry of a for eland basin: the Oligocene Menilite Formation in the Flysch Carpathians of Southern Poland. *Organic Geochemistry*, **29**, 649–669.

Kotarba, M.J. and Koltun, Y.V. 2006. The origin and habitat of hydrocarbons of the Polish and Ukrainian parts of the Carpathian province. In: Golonka, J. and Picha, F.J. (Eds), The Carpathians and their Foreland: Geology and Hydrocarbon Resources. *American Society of Petroleum Geologists Memoir*, **84**, 351–368.

Kováč, M., Nagymarosy, A., Oszczypko, N., Ślączka, A., Csontos, L., Marunteanu, M., Matenco, L. and Márton, E. 1998. Palinspastic reconstruction of the Carpathian–Pannonian region during the Miocene. In: Rakús, M. (Ed.), Geodynamic Development of the Western Carpathians, pp. 189–217. GSSR; Bratislava.

Książkiewicz, M., 1972. Budowa Geologiczna Polski, tom IV. Tektonika, część 3, Karpaty, 228 p. Wydawnictwa Geologiczne; Warszawa.

Kuśmierek, J. 1979. Deformacje grawitacyjne, nasunięcia wsteczne a budowa wgłębna I perspektywy naftowe przedpola jednostki dukielskiej w Bieszczadach. *Prace Geologiczne PAN*, **114**, 1–68.

Latta, D.K. and Anastasio, D.J. 2007. Multiple scale of mechanical stratification and décollement fold kinematics, Sierra Madre Oriental foreland, northeast Mexico. *Journal of Structural Geology*, **29**, 1241–1255.

Laubach S.E, Olson J.E. and Gross M.R. 2009. Mechanical and fracture stratigraphy. *American Association of Petroleum Geologists Bulletin*, **93**, 1423–1426.

Li, F. and Li, W. 2017. Petrological record of CO2 influx in the Dongying Sag, Bohai Bay Basin, NE China. *Applied Geochemistry*, **84**, 373–386.

Liu, N., Liu, L., Qu, X., Yang, H., Wang, L. and Zhao S. 2011. Genesis of authigene carbonate minerals in the Upper Cretaceous reservoir, Honggang Anticline, Songliao Basin: A natural analog for mineral trapping of natural CO_2 storage. *Sedimentary Geology*, **237**, 166–178.

Mastella, L. 1988. Structure and evolution of Mszana Dolna tectonic window, Outer Carpathians, Poland. *Annales So-*

cietatis Geologorum Poloniae, **58**, 53–173. [In Polish with English summary].

Mastella, L. and Rybak-Ostrowska, B. 2012. Tectonic control of tufa occurrences in the Podhale Synclinorium (Central Western Carpathians, southern Poland). *Geological Quarterly*, **56**, 733–744.

Mastella, L. and Szynkaruk, E. 1998. Analysis of the fault pattern in selected areas of the Polish Outher Carpathians. *Geological Quarterly*, **43**, 263–276.

Mastella, M. 1995. Tectonic map of the Fore-Dukla Zone (between Roztoki Dolne and Ustrzyki Górne). Laboratory of Tectonics and Geological Mapping Archive, University of Warsaw; Warsaw.

McLaughlin, R.J., Sorg, D.H., Morton J.L., Theodore T.G., Meyer C.E. and Delevaux, M.H. 1985. Paragenesis and Tectonic Significance of Base and Precious Metal Occurrence along the San Andreas Fault at Point Delgada, California. *Economic Geology*, **80**, 344–359.

Ming, X.R., Liu, L., Yu, L., Bai, H.G., Yu, Z.C., Liu, N., Yang, H.X., Wang, F.G. and Li, B.X. 2017. Thin-film dawsonite in Jurassic coal measure strata of the Yaojie coalfield, Minhe Basin, China: A natural analogue for mineral carbon storage in wet supercritical CO_2. *International Journal of Coal Geology*, **180**, 83–99.

Mitra, S. 1986. Duplex Structures and Imbricate Thrust Systems: Geometry, Structural Position, and Hydrocarbon Potential. *American Association of Petroleum Geologists Bulletin*, **70**, 1087–1112.

Mitra, S. 2002. Fold-accommodation faults. *American Association of Petroleum Geologists Bulletin*, **85**, 671–693.

Mitra, S. 2003. A unified kinematic model for the evolution of detachment folds. *Journal of Structural Geology*, **25**, 1659–1673.

Młynarczyk, M. 1996. Morfologia oraz geochemiczne i tektoniczne warunki powstawania dimanentów marmaroskich w jednostce przeddukielskiej w Bieszczadach. Master thesis, Archives of Laboratorium of Tectonics and Geological Mapping, University of Warsaw; Warsaw.

Moore, J.C. and Vrolijk, P. 1992. Fluids in Accretionary Prisms. *Reviews in Geophysics*, **30**, 113–135.

Morley, C.K. 1994. Fold-generated imbricates: examples from the Caledonides in southern Norway. *Journal of Structural Geology*, **16**, 619–631.

Narębski, W. 1957. O diagenetycznych dolomitach żelazistych w Karpatach fliszowych. *Annales Societatis Geologorum Poloniae*, **26**, 29–50.

Nemčok, M., Krzywiec, P., Wojtaszek, M., Ludhová, L., Klecker, R.A., Sercombe, W.J. and Coward, M.P. 2006. Tertiary development of the Polish and eastern Slovak parts of the Carpathian accretionary wedge: insights from balanced cross sections. *Geologica Carpathica*, **57**, 355–370.

Nemčok, M., Schamel, S. and Gayer R. 2009. Thrustbelts: Structural Architecture, Thermal Regimes, Petroleum Systems, 541 p. Cambridge University Press; Cambridge.

Odling, N.E., Gillespie, P., Bourgine, B., Castaing, C., Chilés, J.-P., Christensen, N.P., Fillion, E., Genter, A., Olsen, C., Thrane, L., Trice, R., Aarsth, E., Walsh, J.J. and Watterson, J. 1999. Variation in fracture system geometry and their implications for fluid flow in fractured hydrocarbon reservoirs. *Petroleum Geoscience*, **5**, 373–384.

Okuyama, Y. 2014. Dawsonite-bearing carbonate veins in the Cretaceous Izumi Group, SW Japan: a possible natural analogue of fracture formation and self-sealing in CO_2 geological storage. *Energy Procedia*, **63**, 5530–5537.

Opolski, Z. 1933. O stratygrafii o paleografii warstw krośnieńskich. *Sprawozdania Państwowego Instytutu Geologicznego*, **7**, 565–636.

Oszczypko, N. 1998. The Western Carpathian Foredeep – development of the foreland basin in front of the accretionary wedge and its burial history (Poland). *Geologica Carpathica*, **49**, 415–431.

Oszczypko, N. 2004. The structural position and tectonosedimentary evolution of the Polish Outer Carpathians. *Przegląd Geologiczny*, **52**, 780–791.

Oszczypko, N. 2006. Late Jurassic–Miocene evolution of the Outer Carpathians fold-and-thrust belt and its foredeep basin (Western Carpathians, Poland). *Geological Quarterly*, **50**, 169–194.

Oszczypko, N. and Tomaś, A. 1985. Tectonic evolution of maginal part of the Polish Flysch Carpathians in the Middle Miocene. *Geological Quarterly*, **1**, 109–128.

Palayangoda, S.S. and Nguyen, Q.P., 2015. Thermal behaviour of raw oil shale and its components. *Oil Shale*, **32**, 160–171.

Pescatore, T. and Ślączka, A. 1984. Evolution models of two flysch basins: the northern Carpathians and the Southern Apennines. *Tectonophysics*, **106**, 49–70.

Poprawa, P., Malata, T. and Oszczypko, N. 2002. Tectonic evolution of the Polish part of Outer Carpathian's sedimentary basins – constraints from subsidence analysis. *Przegląd Geologiczny*, **50**, 1092–1108. [In Polish with English summary]

Preibisch, S., Saalfeld, S. and Tomancak, P. 2009. Globally optimal stitching of tiled 3D microscopic image acquisitions. *Bioinformatics*, **25**, 1463–1465.

Rajchel, J. and Szczepańska, M. 1997. Dolomity żelaziste z warstw krośnieńskich jednostki skolskiej okolic Dynowa. *Zeszyty Naukowe AGH Geologia*, **23**, 229–248.

Ramsay, J.G. 1967. Folding and Fracturing of Rocks, 568 p. McGraw-Hill; New York.

Ramsay, J.G. 1980. The crack-seal mechanism of rock deformation. *Nature*, **284**, 135–139.

Royden, L.H. 1998. Late Cenozoic tectonics of the Pannonian Basin System. In: Royden, L.H. and Horwath, F. (Eds), The Pannonian basin – A study in basin evolution. *American Association of Petroleum Geologists Memoir*, **45**, 27–48.

Rubinkiewicz, J. 1996. Tektonika strefy nasunięcia dukielskiego

w zachodniej części Bieszczadów. *Przegląd Geologiczny*, **44**, 1199–1204.

Rubinkiewicz, J. 1998. Development of joints in Silesian nappe (Western Bieszczady, Carpathians, SE Poland). *Przegląd Geologiczny*, **46**, 820–826. [In Polish with English summary]

Rubinkiewicz, J. 2000. Development of fault pattern in the Silesian Nappe: Eastern Outer Carpathians, Poland. *Geological Quarterly*, **44**, 391–403.

Rubinkiewicz, J. 2007. Fold-thrust-belt geometry and detailed structural evolution of the Silesian nappe – eastern part of the Polish Outer Carpathians (Bieszczady Mts.). *Acta Geologica Polonica*, **57**, 479–508.

Rybak, B. 2005. Structural analysis of selected fragments of thrust fault zones of the Magura Unit and Fore-Dukla Zone in the Polish Outer Carpathians, 106 p. PhD thesis, Warsaw University; Warsaw. [In Polish]

Rybak-Ostrowska, B., Konon, A., Domonik, D., Poszytek, A. and Uroda, J., 2017. Shallow generated damage within non-planar strike-slip fault zones – role of sedimentary rocks in slip accommodation, SW Holy Cross Mountains, Poland. *International Journal of Earth Sciences*, **106**, 1863–1888.

Schindelin, J., Arganda-Carreras, I. and Frise, E. 2012. Fiji: an open-source platform for biological-image analysis. *Nature Methods*, **9**, 676–682.

Scholz, C.H 1988. The brittle-plastic transition and the depth of seismic faulting. *Geologische Rundschau*, **77**, 319–328.

Scholz, C.H. 2002. The Mechanics of Earthquakes and Faulting, 467 p. Cambridge University Press; Cambridge.

Shackleton, J.R., Cook, M.L. and Susman, A.J. 2005. Evidence for temporally changing mechanical stratigraphy and effects on joint-network architecture. *Geology*, **33**, 101–104.

Sibson, R.H. 1977. Fault rocks and fault mechanisms. *Journal of Geological Society of London*, **133**, 191–213.

Sibson, R.H. 1983. Continental fault structure and the shallow earthquake source. *Journal of Geological Society of London*, **140**, 741–767.

Sibson, R.H. 1996. Structural permeability of fluid driven fault-fracture meshes. *Journal of Structural Geology*, **18**, 1031–1042.

Sibson, R.H. 2003. Brittle-failure controls on maximum sustainable overpressure in different tectonic regimes. *American Association of Petroleum Geologist Bulletin*, **87**, 901–908.

Sirbescu, M.-L. and Nabelek, P.I. 2003. Crustal melts below 400ºC. *Geology*, **31**, 685–688.

Ślączka, A. 1957. Geological Map of Poland, Bukowsko sheet, scale 1:50000. Wydawnictwa Geologiczne; Warszawa.

Ślączka, A. 1958. Notes on the geological position of mineral ores in the region of Baligród (Middle Carpathians). *Geological Quarterly*, **2**, 637–643. [In Polish with English summary]

Ślączka, A. 1959. Stratigraphy of the Silesian series of the Bystre slice (to the south of Baligród). *Biuletyn Instytutu Geologicznego*, **131**, 202–260. [In Polish with English summary]

Ślączka, A. 1968. Explanation to the Geological Map of Poland, Bukowsko sheet, scale 1:50000. Wydawnictwa Geologiczne; Warszawa.

Ślączka, A. 1971. The geology of the Dukla Unit. *Prace Instytutu Geologicznego*, **63**, 1–76. [In Polish with Russian and English summary]

Ślączka, A. and Żytko and K., 1978. Geological Map of Poland, sheet Łupków, scale 1:200000. Wydawnictwa Geologiczne; Warszawa.

Smith, J.W. and Milton, C. 1966. Dawsonite in the Green River formation of Colorado. *Economic Geology*, **61**, 1029–1042.

Stevenson, J. and Stevenson, L.S. 1965. The petrology of dawsonite at the type locality, Montreal. *Canadian Mineralogist*, **8**, 249–252.

Stoica, G. and Pérez-Ramírez, J. 2010. Stability and Inter-conversion of synthetic dawsonite in aqueous media. *Geochimica et Cosmochimica Acta*, **74**, 7048–7058.

Suppe, J. and Medwedeff, D.A. 1990. Geometry and kinematics of fault propagation folding. *Eclogae Geologicae Helvetiae*, **83**, 409–454.

Świdziński, H. 1958. Geological Map of Polish Carpathians, eastern part, scale 1:200000. Wydawnictwa Geologiczne; Warszawa.

Świerczewska, A. 2005. The interplay of the thermal and structural histories of the Magura Nappe (Outer Carpathians) in Poland and Slovakia. *Mineralogia Polonica*, **36**, 91–144

Szczepańska, M. 2003. Konkrecje węglanowe jednostki skolskiej. *Gospodarka Surowców Mineralnych*, **19**, 5–33.

Tołwiński, K. 1933. Centralna Depresja Karpacka. *Geologia i Statystyka Naftowa Polski*, **7**, 362–366.

Trémosa, T.J., Castillo, C., Vong, C.Q., Kervévan, C., Lassin, A. and Audiganeremosa, P. 2014. Long-term Assessment of Geochemical Reactivity of CO_2 Storage in Highly Saline Aquifers: Application to Ketzin, in Salah and Snøhvit storage sites. *International Journal of Greenhouse Gas Control*, **20**, 2–26.

Van Noten K., Van Baelen H. and Sintubin M. 2012. The complexity of 3D stress-state changes during compressional tectonic inversion at the onset of orogeny. *Geological Society, London, Special Publications*, **367**, 51–69.

Vergés, J., Goodarzi, M.G.H., Emami, H., Karpuz, R., Efstathiou, J. and Gillespie, P. 2011. Multiple Detachment Folding in Pusht-e Kuh Arc, Zagros: Role of Mechanical Stratigraphy. In: McClay, K., Shaw, J.H. and Suppe, J. (Eds), Thrust fault-related folding. *American Association of Petroleum Geologists Memoir*, **94**, 69–94.

Wigley, M., Kampman, N., Dubacq, B. and Bickle, M. 2012. Fluid-mineral reactions and trace metal mobilization in an exhumed natural CO_2 reservoir, Green River, Utah. *Geology*, **40**, 555–558.

Woodcock, N.H. and Mort, K. 2008. Classification of fault

breccias and related fault rocks. *Geological Magazine*, **145**, 435–440.

Worden, R.H. 2006. Dawsonite cement in the Triassic Lam Formation Shabwa Basin, Yemen: a natural analogue for a potential mineral product of subsurface CO_2 storage for greenhouse gas reduction. *Marine and Petroleum Geology*, **23**, 61–77.

Yu, M., Liu, L., Yang, S., Yu, Z., Li, S., Yang, Y. and Shi X. 2016. Experimental identification of CO_2-oil-brine-rock interactions: Implications for CO_2 sequestration after termination of a CO_2-EOR project. *Applied Geochemistry*, **75**, 137–151.

Zalba, P.E., Conconi, M.S., Morosi M., Manassero, M. and Comerio, M. 2011. Dawsonite in tuffs and litharenites of the Cerro Castaño Member, Cerro Barcino Formation, Chubut Group (Cenomanian), Los Altares, Patagonia, Argentina. *Canadian Mineralogist*, **49**, 503–520.

Zerai, B., Saylor, B.Z. and Matisoff, G. 2006. Computer simulation of CO_2 trapped through mineral precipitation in the Rose Run Sandstone, Ohio. *Applied Geochemistry*, **21**, 223–224.

Żytko, K., Zając, R., Gucik, S., Ryłko, W., Oszczypko, N., Garlicka, I., Nemčok, J., Eliaś, M., Menčik, E. and Stranik, Z. 1989. Map of the tectonic elements of the Western Outer Carpathians and their foreland, 1:500 000. In: Poprawa, D. and Nemčok, J. (Eds), Geological Atlas of the Western Outer Carpathians and their Foreland. Państwowy Instytut Geologiczny; Warszawa.

Manuscript submitted: 7th March 2019
Revised version accepted: 23rd September 2019